3D INTEGRAL FIELD OBSERVATIONS OF TEN GALACTIC WINDS – I. EXTENDED PHASE (≳10 MYR) OF MASS/ENERGY INJECTION BEFORE THE WIND BLOWS

R.G. Sharp[1] and J. Bland-Hawthorn[2,3]
Draft version January 25, 2010

ABSTRACT

In recent years, we have come to recognize the widespread importance of large-scale winds in the lifecycle of galaxies. The onset and evolution of a galactic wind is a highly complex process which must be understood if we are to understand how energy and metals are recycled throughout the galaxy and beyond. Here we present 3D spectroscopic observations of a sample of 10 nearby galaxies with the AAOmega-SPIRAL integral field spectrograph on the 3.9m AAT, the largest survey of its kind to date. The double-beam spectrograph provides spatial maps in a range of spectral diagnostics: [O III]5007, Hβ, Mg b, Na D, [O I]6300, Hα, [N II]6583, [S II]6717, 6731. We demonstrate that these flows can often separate into highly ordered structures through the use of ionisation diagnostics and kinematics. All of the objects in our survey show extensive wind-driven filamentation along the minor axis, in addition to large-scale disk rotation. Our sample can be divided into either starburst galaxies or active galactic nuclei (AGN), although some objects appear to be a combination of these. The total ionizing photon budget available to both classes of galaxies is sufficient to ionise all of the wind-blown filamentation out to large radius. We find however that while AGN photoionisation always dominates in the wind filaments, this is not the case in starburst galaxies where shock ionisation dominates. This clearly indicates that after the onset of star formation, there is a substantial delay (≳ 10 Myr) before a starburst wind develops. We show why this behavior is expected by deriving "ionisation" and dynamical timescales for both AGNs and starbursts. We establish a sequence of events that lead to the onset of a galactic wind. The clear signature provided by the ionisation timescale is arguably the strongest evidence yet that the starburst phenomenon is an impulsive event. A well-defined ionisation timescale is not expected in galaxies with a protracted history of circumnuclear star formation. Our 3D data provide important templates for comparisons with high redshift galaxies.

Subject headings: Galaxies: individual (NGC 253, NGC 1365, NGC 1482, NGC 1808, NGC 3628, NGC 5128, Circinus, NGC 6240, NGC 6810, IC 5063)

1. INTRODUCTION

Recent observations reveal that outflows are important in the lifecycle of galaxies. First, Tremonti *et al.* (2004) find evidence for chemical enrichment trends throughout star-forming galaxies over three orders of magnitude in stellar mass. Surprisingly, the enrichment trends are observed to continue all the way down to $\log(L_{\rm bol}/L_\odot) \approx 4$ (Kirby *et al.* 2008) where $L_{\rm bol}$ is the bolometric luminosity of the galaxy. Indeed, there is evidence that galaxies that exceed the mass of the Milky Way manage to retain a large fraction of their metals, in contrast to lower mass galaxies where metal loss appears to be anticorrelated with baryonic mass. Recent theoretical work has shown that a low-metal content in dwarf galaxies is attributable to efficient metal-enriched outflows (Dalcanton 2007). Secondly, there is now strong evidence for large-scale outflows in the Galaxy across the electromagnetic spectrum (Bland-Hawthorn & Cohen 2003; Fox *et al.* 2005; Keeney *et al.* 2006). Finally, the intergalactic medium (IGM) at all redshifts shows signs of significant metal enrichment

consistent with the action of winds (Cen & Ostriker 1999; Madau *et al.* 2001; Ryan-Weber *et al.* 2006; Davé *et al.* 2008). A high proportion of Lyman break galaxies at $z \sim 3 - 4$ show kinematic signatures of winds (Erb *et al.* 2006) as do many nearby dwarf starbursts (Schwartz & Martin 2004) and ultraluminous infrared galaxies (Martin 2006; Schwartz, Martin, Chandar *et al.* 2006).

N-body simulations of galaxy formation within cold dark matter (CDM) cosmology fail to produce realistic galactic disks (Navarro & White 1994; Steinmetz & Müller 1995). Over-cooling in CDM+hydrodynamic simulations, due primarily to a lack of resolution, results in too much gas arriving in the centre of the galaxies. But a useful aspect of these incomplete models has been to highlight the possible role of feedback in shaping galaxies. Vigorous feedback in the early phase of galaxy formation is a partial solution to the angular momentum problem by preventing baryons from losing too much of their specific angular momentum through the interaction with dark matter (Fall 2002). Indeed, some authors have claimed more realistic disks retaining much more of their angular momentum when one includes the action of AGN-driven jets (Robertson *et al.* 2006) or starburst driven winds (Efstathiou 2000).

Our new survey is preempted by a vast literature across a broad spectrum that can be traced back over two decades − comprehensive reviews are given by Heckman *et al.* (1989) and Veilleux *et al.* (2005). Much of

rgs@aao.gov.au
jbh@physics.usyd.edu.au
[1] Anglo-Australian Observatory, PO Box 296, Epping, NSW 1710, Australia
[2] Sydney Institute for Astronomy, School of Physics A28, University of Sydney, NSW 2006, Australia
[3] Leverhulme Visiting Professor, Physics Department, University of Oxford, 1 Keble Rd, Oxford, OX1 3RH, UK

the early optical work on galactic outflows was limited to narrowband images and long-slit spectroscopy (e.g. McCarthy *et al.* (1987); Heckman, Armus & Miley (1990); Phillips (1993); Lehnert & Heckman (1996)) although Fabry-Perot observations have been carried out in a few emission lines (e.g. Bland & Tully (1988); Cecil (1990)). The quality of UV, x-ray, infrared and radio continuum observations has greatly improved in recent years (e.g. Hoopes *et al.* 2005; Strickland *et al.* 2004; Grimes, Heckman, Aloisi *et al.* (2009)). Even without the kinematic separation of compound emission structures that is possible via spectroscopy, there are clear associations between these bands and the optical maps (e.g. Veilleux *et al.* 1994; Cecil *et al.* 2002). Historically, most winds had been confirmed kinematically from evidence of line-splitting along the galaxy minor axis, but at least one wind has been discovered through its ionisation signature (Veilleux & Rupke 2002). In recent times measurement of blueshifted absorption lines have proved powerful in this regard.

In this new study, we perform wide field integral field spectroscopy of a sample of nearby galactic winds. The advantages offered by a wide wavelength base line and moderate spectral resolutions allow the determination of physical parameters for wind outflow mechanics based on ionisation and kinematic signatures e.g. rotating disk, high-latitude warm ionizing medium, wind filaments, entrained gas. One well-studied object in particular convinced us of the potential for wide-field mapping with an integral field spectrograph. The projected distribution of optical line emission in M82 is exceedingly complex but with the aid of Fabry-Perot observations, Shopbell & Bland-Hawthorn (1998) were able to kinematically separate the front side from the back side of the wind flow, and from the diffuse halo of broadened line emission (see also the recent IFS studies of Westmoquette, Smith, Gallagher *et al.* (2009); Westmoquette, Gallagher, Smith *et al.* (2009)). When this is done, both the ionisation and kinematics exhibit well ordered behavior. The lesson is clear: with complete observations, it is possible to separate distinct dynamical components. Only then does it become possible to determine physical parameters for the outflow mechanism.

In this first paper, we present the new observations and describe the reduction procedures specific to integral field spectroscopy ($\S$ 2). We present emission-line flux and line ratio maps for a wide range of diagnostics (e.g. ionisation and density). For each galaxy, we use the ionisation diagnostic diagrams (IDDs) to delineate the different sources of ionisation as a function of location and ionisation source (see $\S$ 3) and classify the sample targets according to their individual IDDs ($\S$ 3.1 - starbursts & $\S$ 3.2 - AGN). These diagnostic diagrams reveal well-ordered behavior across each galaxy. In $\S$ 4 we consider the source of ionisation from a theoretical perspective and use these considerations to construct an evolutionary sequence for galactic winds in section $\S$ 5. Our conclusions are presented $\S$ 6.

Through this work, we assume a flat concordance cosmology such that H_o=71 km s^{-1} Mpc^{-1}, Ω_M=0.27 and Ω_Λ=0.73.

2. OBSERVATIONS AND DATA REDUCTION

2.1. *Observing set up and procedure*

The AAOmega integral-field spectrograph at the AAT 3.9m is ideally suited to our study (see Appendix). The SPIRAL integral field unit (IFU) is a 32×16 element rectangular microlens array coupled via an optical fibre feed to the dual beam AAOmega spectrograph (Saunders *et al.* 2004; Sharp *et al.* 2006). Mounted at the Cassegrain auxilliary focus, the 0.7″ IFU pixel scale is well matched to the typical seeing at the AAT, and gives excellent sensitivity to extended low surface brightness features. The single pointing field-of-view is 22.4″×11.2″. High accuracy, guide-probe offset guiding allows simple and reliable mosaicing of large areas. The default position angle of the IFU places the long axis in an east-west direction. Observations of a number of targets were undertaken at alternate PAs to accommodate the demands of other observing programs undertaken alongside the observations reported here.

Observations were undertaken over a number of observing runs as detailed in Table 1. The dual beam AAOmega spectrograph provides excellent coverage of the spectral features of interest, while maintaining a high spectral resolution. We observe with the 1500V and 1000R Volume Phase Holographic (VPH) gratings in the blue and red arms respectively. We use a 5700Å dichroic beam splitter and center the wavelength coverage and VPH blazes at 5000Å and 6800Å, resulting in 2.4 pixel mid-range resolution elements of R~6300 and R~5600 (velocity resolutions of $\approx$ 35 and $\approx$50 km s^{-1} FWHM). On accounting for the sample redshift range, this targets the emission lines Hβ/[O III] in the blue and [O I]/Hα/[N II]/[S II] in the red. Unfortunately the important [O II] doublet at 3727Å falls outside of the observable spectral range with the chosen settings. We consider this to be a crucial line for future studies of this kind.

Quartz-Halogen flatfield exposures and CuAr+FeAr arc lamp exposures are taken at intervals throughout the observation to allow fibre tracing on the CCDs (both arms of AAOmega use E2V 2k×4k CCDs), flat fielding and wavelength calibration. Stationed in the west Coudé room, AAOmega is kept thermally and gravitationally stable throughout each night's observations in order to minimize the overhead on system calibrations. The strong night sky oxygen line at 5577Å falls outside the observed range and so cannot be used to calibrate relative fibre transmission as is the common practice in low resolution multi-object spectroscopy. Therefore twilight flatfield frames are observed in order to account for relative fibre-to-fibre transmission variations.

An assortment of spectrophotometric standard stars[4] were observed throughout each observing block, in order to prepare a flux calibration solution. The scatter in the calibration function derived from the standards during the observations indicates a 10% uncertainty in the absolute flux calibration level. The relative calibration with wavelength, a quantity more relevant to line ratio determinations, is consistent at the ~2-3% level, as determined from the comparison of calibration observations

---

[4] Spectrophotometric standard stars were chosen from the ESO spectrophotometric standard list available at http://www.eso.org/sci/observing/tools/standards/spectra/

TABLE 1
A summary of AAT observations with the
AAOmega−SPIRAL spectrograph.

Observing Dates	Objects Observed
May 2007	NGC 3628, NGC 6810, NGC 5128(CenA)
October 2007	NGC 1365, NGC 1482, NGC 1808
July 2008	Circinus, NGC 253, IC 6063
August 2008	NGC 6810, NGC 1705, NGC 6240

over the course of the survey.

Each target was observed as part of a multi-pointing mosaic. An overlap of 1 or 2 IFU elements ($0.7''$ or $1.4''$) was allowed to enable relative intensity scaling and accurate mosaicing of the final data sets. Individual science exposures were typically 1200 sec. Mosaic sizes vary between galaxies, but are typically of the order of six to twelve IFU positions, yielding mosaics of the order $20''$ to $60''$ on a side.

Since our targets completely fill each IFU pointing, it is not possible to generate a sky subtraction solution from fibres within each IFU pointing. To achieve accurate sky subtraction, a small number of dedicated offset sky frames was taken each night. Data was processed in real time at the telescope using the 2dfdr software package. This allowed monitoring of the observing conditions such that the mosaic pattern could be repeated or adapted if required. The final data analysis was carried out using a custom suite of IDL routines.

There are four isolated "dead elements" within the SPIRAL IFU. During the reduction process, these are replaced with the average spectrum of the four adjacent IFU elements prior to mosaicing the data. Individual frames were then aligned and mosaiced using telescope offset information and a suite of custom written software tools. Frames are scaled, based on an iterative comparison of overlap regions in the mosaic, in order to account for minor variations in transparency, seeing and exposure time.

2.2. The sample

We targetted a sample of ten galaxies with known galactic winds (Veilleux *et al.* 2003; Heckman *et al.* 1990; Lehnert & Heckman 1996). The details of the sources are presented in Table 2. Given that the aim of our study is to compare the properties of AGN vs. starburst winds, we did not include a "control" sample of non-wind galaxies. Integral field observations are extremely time consuming and indeed IFU surveys of galaxies have rarely been attempted before. Notable examples are the SAURON survey of early type galaxies (e.g. de Zeeuw *et al.* 2002) and the SINS survey at higher redshift (Genzel *et al.* 2008).

We limit our survey to southern hemisphere sources with bolometric luminosities in the range $L_{\rm bol} = 1-10 \times 10^{10}~L_\odot$ to ensure the impact of photoionisation by the central source (whether starburst or AGN) is detectable out to large galactocentric distances. (The physical motivation for this statement is given in §4.1.) With a view to going after a lower luminosity sample, we attempted a preliminary study of the dwarf galaxy NGC 1705 (Annibali, Greggio, Tosi *et al.* 2003; Meurer, Freeman, Do-

pita & Cacciari 1992; Hunter, Hawley & Gallagher 1993). Our initial observations (not presented here) served to emphasize that low mass galaxies typically have lower metallicities which render many of the ionisation diagnostics intrinsically weak. A survey sample of a substantial number of low-luminosity wind sources ($\gtrsim 10$) will require a suitable IFU spectrograph on an 8m class telescope.

For each of the ten wind galaxies, the SPIRAL IFU was used in a simple tiling pattern to cover most of the filamentary emission above a surface brightness of 1×10^{-17} erg cm^{-2} s^{-1} arcsec^{-2} (cgs). The SPIRAL mosaic patterns (or footprints) are overlayed on *HST*/WFPC2 imaging data in Fig. 1. WFPC2 images have been used for all sources with the exception of NGC 1482 for which *UKST* data from the Digitized Sky Survey has been used. The *HST*/WFPC2 data were obtained from the Multimission Archive at the Space Telescope Science Institute (MAST). Fig. 1 emphasizes the need for much wider field IFUs for the study of nearby galaxies. While these are under development in Europe and Australia, we stress the simultaneous requirements of spectral coverage and resolution (see Appendix) which are often sacrificed in order to achieve a larger spatial format. In this respect, we consider the AAOmega-SPIRAL spectrograph to be ideal for the proposed science, even with the limited field of view.

2.3. Emission line maps

Emission line maps are constructed via profile fitting to each individual spectrum from the data cubes. Lines are approximated with single Gaussian profiles in the work that follows, and each line is fitted independently, rather than simultaneously, which is possible at the SPIRAL resolution in most instances. This simplification overlooks effects such as line splitting observed in emission from the front and back surfaces of an outflow cone and asymmetric profiles (blue/red shoulders to emission lines) from marginally resolved kinematic components. Ultimately a full deconvolution of each data cube, informed by kinematic models for each source, will be required (e.g. Westmoquette, Smith, Gallagher *et al.* (2009)).

Currently no account is being taken for the underlying stellar absorption although Hβ absorption is evident close to the disk in some cases. The limited wavelength coverage, which excludes Balmer lines higher than Hβ, hampers a proper treatment of the underlying stellar continuum. The dominant effect of neglecting stellar absorption will be to underestimate the flux in the Hβ emission line, suggesting that [O III]/Hβ ratios may be moderately overestimated in regions with a significant contribution from stellar continuum. In our present study, Balmer absorption has negligible impact since we are concerned with filaments that extend beyond the projected stellar disk.

2.4. Ionisation diagnostic diagrams

For each object, we construct "ionisation diagnostic diagrams" (IDDs) as prescribed by Baldwin, Phillips & Terlevich (1981) and Veilleux & Osterbrock (1987) for different families of optical emission lines. An example, constructed from the observations of NGC 1482 (Figs. 2

TABLE 2
The target sample of southern or equatorial galactic wind sources.

Object	RA/Dec (J2000)	Redshift	Hubble type[1]	Spec class[2]	i	M_B	L_{Bol}[3]	R/Mpc	kpc/arcsec
NGC 253	00 47.6 −25 18	0.00081	Sc(X)	Hɪɪ	86	−20.02	2.8	2	0.017
NGC 1365	03 33.7 −36 08	0.00546	Sb(B)	Hɪɪ, Sy2	63	−21.26	9.3	16.9	0.100
NGC 1482	03 54.7 −20 30	0.00639	Sa(P)	Hɪɪ	58	−18.89	1.1	19.6	0.121
NGC 1808	05 07.7 −37 31	0.00332	SO/a(X)	Hɪɪ, Sy2?	50	−19.52	2.2	10.8	0.059
NGC 3628	11 20.3 +13 37	0.00281	Sb(P)	Hɪɪ, LINER	87	−19.96	2.8	7.7	0.041
NGC 5128	13 25.3 −43 01	0.00183	SO, Lenticular	Sy2	43	−20.97	8.5	4.9	0.053
Circinus	14 13.2 −65 20	0.00145	Sb(A)	Sy2	65	−21.23	9.0	4.2	0.014
NGC 6240	16 53.0 +02 24	0.02445	I0	LINER, Sy2	—	−21.30	8.2	—	0.5
NGC 6810	19 43.6 −58 40	0.00678	Sa(A)	Hɪɪ, Sy2?	82	−20.61	5.5	25.3	0.135
IC 5063	20 52.0 −57 04	0.01135	Sa	Sy2	—	−20.34	4.2	—	0.22

Note 1: Vizier database at http://vizier.u-strasbg.fr/
Note 2: NED database at http://nedwww.ipac.caltech.edu/; a question mark indicates that the Seyfert classification has been questioned in later studies.
Note 3: Bolometric luminosities, L_{Bol}, in units of 10^{10} $L_{\odot}$, are computed from the modeling of Buzzoni (2005), with uncertainties of typically 10% for different assumed ages of the stellar population over the full range 1-14 Gyr.

TABLE 3
Classification of the ionisation mechanism for the galactic wind emission.

Object	[O ɪɪɪ] & [N ɪɪ]	[O ɪɪɪ] & [S ɪɪ]	[O ɪɪɪ] & [O ɪ]
Starbursts			
NGC 253	10:90	10:90	10:90
NGC 1482	10:90	10:90	10:90
NGC 1808	20:80	0:0	0:0
NGC 3628	0:0[1]	—	—
NGC 6810	0:0[1]	0:0	—
AGNs			
NGC 1365	90:10	90:10	100:0
NGC 5128	50:50	0:100	60:40
Circinus	100:0	60:40	100:0
NGC 6240	—	—	—
IC 5063	100:0	90:10	100:0

The primary ionisation source in the galactic wind-driven filaments is determined from the IDDs in Figs. 4,7,10,12,15,18,21,24 & 28. For each of the IDDs, we show the percentage of points (AGN:Shock) outside of the maximal star formation boundary (Kewley *et al.* 2001) consistent with the fiducial models derived from NGC 1365 and NGC 1482. Reliable fractions are hard to derive so the numbers shown are indicative. A ratio of 0:0 indicates that all emission is contained within the star formation boundary. Blank entries indicate that the IDD could not be constructed in the given line ratio.
Note 1: Figs. 12 and 14 clearly delineate enhanced [N ɪɪ]/Hα co-spatial with line profile splitting in the outflowing gas, consistent with the shock signatures seen in NGC 1482 (see §3.1).

& 3), is presented in Fig. 4. We have included the *extreme starburst* model of Kewley *et al.* (2001) as a common fiducial indicator. The IDDs for the galaxy sample are presented in Figs. 4, 7, 10, 15, 18, 21, 24 & 28.

We have added two further reference lines to each diagnostic plot, which are derived from two objects in our sample. The two diagonal lines across the IDDs indicate the different tracks traced by the bulk of the data points in NGC 1365 and NGC 1482. These two galaxies are the clearest examples within our sample of AGN photoionisation (Veron, Lindblad, Zuiderwijk *et al.* 1980) and shock ionisation (Veilleux & Rupke 2002) respectively. As such, these tracks constitute our own internal calibration of two very different sources of gaseous ionisation and al-

low for a very precise differential analysis for our galaxy sample. This clear distinction arising from the IDDs for each galaxy allows us to cleanly separate most of the galaxies into one or other category in terms of the dominant source of ionisation in the outer filaments.

We emphasize that shock diagnostics can overlap a region of the IDDs occupied by so-called LINER objects, some of which may be excited by dilute photoionizing sources rather than by shocks. The origin of LINER ionization is still somewhat controversial. For all of our objects, the strength of the [NII], [SII] and [OIII] lines, and sometimes [OI] lines, argues against "LINER" ionization so we do not consider it here.

3. THE GALAXY SAMPLE

We provide an overview of each galaxy based on an extensive literature review with particular emphasis on recent work. Our initial classification below in terms of starburst or AGN is taken from Table 2. We start with the canonical objects NGC 1482 and NGC 1365 in each category respectively.

3.1. *Starbursts*

NGC 1482

Hameed & Devereux (1999) first reported "filaments and chimneys of ionised gas" in NGC 1482. More recently, tunable filter observations of NGC 1482 led Veilleux & Rupke (2002) to consider it the prime example of a "shock excited, limb-brightened conic wind structure". No compelling evidence for an AGN has yet been reported in the literature at any wavelength and thus NGC 1482 is classified as a typical Hɪɪ galaxy (Kewley *et al.* 2001).

Our SPIRAL IFU observations of NGC 1482 are presented in Figs. 2−4. The conic outflow structure seen in the emission-line gas (Veilleux & Rupke 2002) and diffuse x-ray emission (Strickland *et al.* 2004a) is evident in the SPIRAL integrated line flux maps (Fig. 2). The enhanced line emission in the forward facing component of the limb brightened bi-cone is clearly visible above the disk (particularly towards the bottom of the [N ɪɪ] and [O ɪɪɪ] maps of Fig. 2) with the counter cone visible, subject to dust attenuation, below the inclined disk in

TABLE 4
SPATIAL EXTENT AND BRIGHTNESS OF THE EMISSION-LINE GAS.

Object	$L_{\rm Bol}$ $(10^{10}\,\mathrm{L_\odot})$	Extent (arcsec)	Deprojected (kpc)	$\mu(\mathrm{H}\alpha)$ @ 1 kpc $(\mathrm{ergs\,s^{-1}\,cm^{-2}\,arcsec^{-2}})$	$L(\mathrm{H}\alpha)$ @ 1 kpc $(\mathrm{ergs\,s^{-1}\,arcsec^{-2}})$
NGC 253	2.8	30.5	0.5	3.8e-16 ± 4.6e-16	5.4e+35 ± 6.5e+35
NGC 1365	9.3	16.4	1.8	2.6e-16 ± 1.2e-16	1.4e+37 ± 6.5e+36
NGC 1482	1.1	15.5	2.2	8.9e-16 ± 4.4e-16	6.6e+37 ± 3.3e+37
NGC 1808	2.2	22.5	1.7	1.6e-16 ± 5.1e-17	3.7e+36 ± 1.2e+36
NGC 3628	2.8	28.0	0.4	5.2e-17 ± 2.2e-17	1.7e+36 ± 6.9e+35
NGC 5128	8.5	36.0	2.8	4.7e-16 ± 2.2e-16	6.8e+36 ± 3.2e+36
Circinus	9.0	24.6	0.4	1.9e-16 ± 8.5e-17	1.5e+36 ± 6.6e+35
NGC 6810	5.5	12.0	16.4	5.5e-16 ± 2.4e-16	4.7e+37 ± 2.1e+37
IC 5063	4.2	6.0	1.4	1.3e-15 ± 5.3e-16	3.1e+38 ± 1.3e+38

The spatial extent of emission-line gas is estimated from measurements of the Hα and [N II] emission along the minor axis of each galaxy. The point at which line fitting becomes unreliable is determined for each mosaic. For the default observing mode, this corresponds to a line surface brightness of 2×10^{-17} cgs. The physical extent within the mosaics is corrected for the galactic inclination given in Table 2. In the final two columns, we give the mean Hα surface brightness and the mean Hα luminosity at 1 kpc (with 1σ uncertainties), or at the physical limit of the gas if this is less than 1 kpc. These values are not corrected for internal dust extinction.

most emission lines. Line profiles from the near and far side of the extended filaments show clear evidence of line splitting at the level of ~130 km s^{-1}.

Strong line emission is seen throughout the galactic disk with the base of the outflow cone coincident with the outer boundary of strong star formation (as measured by the gradient in the Hα emission along the disk), indicative of a wind launched above (and below) the plane of the disk from an extended starburst region. A sharp gradient in the electron density, as measured by the [S II]:[S II] ratio (Fig. 3) is also coincident with the boundaries of the base of the outflow region, suggestive of a clearing of the inner disk by the action of the starburst wind.

Under an alternate intensity scaling, the Hα integrated flux map does show a compact nuclear region at the limit of the spatial resolution of the SPIRAL data. The nucleus appears to be resolved at mid-IR wavelengths (Siebenmorgen *et al.* 2008) and with no spectroscopic evidence of an AGN the emission is likely that of a compact star forming region.

The line ratio diagnostics for NGC 1482 are shown in Fig. 4. The limited sensitivity to [O III] emission, particularly in the counter flow region to the north of the disk (presumably hampered by significant dust attenuation) restricts the region that can be analysed in this manner. As for all of our sample, most of the data points are bunched to the right of the IDD, consistent with metal enriched gas in the nuclear regions of massive galaxies. The body of the disk emission is consistent with high metallicity star formation (Z>1.0, Kewley *et al.* (2001)).

The emission from the bi-cone of NGC 1482 is compatible with shock-induced ionisation (Veilleux & Rupke 2002). The line ratios *harden* with increasing height above the disk place. This could indicate the gas becomes increasingly shocked at greater distance above the disk (not unexpected since the wind speed will increase with reduced ISM gas density (Rand 1998)), or may simply be a product of dilution of the outflow emission line components blended with the underlying disk emission in the simple single Gaussian line apporoximation currently implemented. The line ratio maps indicate harder line ratios on the western side of the southern lobe, coincident with the x-ray emitting gas presented by Strickland

et al. (2004b).

NGC 253

Due to its proximity, NGC 253 is one of the best studied examples of the class of luminous infrared galaxies known to be undergoing an intense burst of star formation (Rieke, Lebofsky, Thompson *et al.* 1980). Demoulin & Burbidge (1970) interpreted the disturbed kinematics of the emission line gas as a conic outflow which was later shown (McCarthy, van Breugel & Heckman 1987) to be qualitatively consistent within the Chevalier & Clegg (1985) starburst wind model. Evidence for entrainment of molecular gas within the outflow has been reported (Sakamoto *et al.* 2006). The outflow is clearly visible in the UV although the observed flux is most likely light from the central starburst scattered by dust entrained in the outflow (Hoopes *et al.* 2005). X-ray observations do not reveal evidence for an AGN, being consistent with a starburst driven galactic wind (Persic *et al.* 1998; Strickland *et al.* 2000).

The large spatial extent of NGC 253 meant that only the southern side of the galactic plane could be surveyed with the SPIRAL IFU in the allocated observing time (~4 hours per object). The observations are presented in Figs. 5−7. NGC 253 closely follows the emission pattern of NGC 1482. Two prominent fingers of emission, interpreted as the limb brightened edges of a line-emitting cone, are clearly identified in the SPIRAL data (Figs. 5), with the structure most clearly highlighted by the contours of [N II] emission. Like M82, the [O III] emission is more centrally condensed than the low ionisation emission (cf. Shopbell & Bland-Hawthorn 1998). Much like in NGC 1482, the prominence of the [N II] emission is suggestive of shock excitation at the boundary of the flow.

Line splitting, indicative of a hollow conic outflow structure, is seen in spectra taken from the central region of the outflow above the plane of the disk. The velocity separation is roughly ~100 km s^{-1} close to the disk but rises to >230 km s^{-1} at the edge of the IFU mosaic suggesting an acceleration of the outflow with increasing height above the disk plane (under the assumption of a constant cone opening angle). The limb brightened cone edges show only a single velocity component. The wind

filaments converge to a considerably more compact region (~ 140 pc) in the nuclear disk compared to what is seen in NGC 1482.

Consistent with Strickland *et al.* (2000), the western limb is brighter in the Balmer lines. In contrast, we find that the eastern limb is consistently brighter in all forbidden lines relative to Hα (Fig. 6). A similar asymmetry is seen in NGC 1482. We observe an apparent hardening of the line ratios with height above the disk, but this may be due to dilution from the inner disk.

The IDDs constructed from the SPIRAL data (Fig. 7) reveal the dominance of shock ionisation in the optical filaments. In particular, weak [O I] emission is observed across the cone being especially prominent in the eastern limb. At large distances, the weaker [O I] emission is compromised by the proximity of strong telluric [O I] emission due to the low redshift of NGC 253.

Consistent with this picture, Strickland *et al.* (2000) conclude that the outflow emission seen at x-ray energies is derived from a low filling factor gas that is excited by interaction between the wind and the ISM on the surface of the outflow cone, rather than from the wind itself. In conclusion, NGC 253 exhibits a starburst driven, shock excited wind nebula, observed in this instance only on the near side of the disk due to the spatial coverage of the data. The wind originates from a centrally confined starburst, rather than from a significant portion of the disk region.

NGC 1808

The "peculiar" nuclear spectrum of this object led Veron-Cetty & Veron (1985) to classify NGC 1808 as a weak Seyfert 2 galaxy. Subsequent observations (Forbes, Boisson & Ward 1992) showed that the properties of the nuclear emission are more plausibly explained by a nuclear starburst, a view supported by mid-IR diagnostics (Laurent *et al.* 2000). Phillips (1993) confirm the nuclear outflow suspected from earlier work, arguing against the Seyfert 2 identification in favour of a starburst-driven outflow source.

Junkes *et al.* (1995) find that the nuclear x-ray emission from the unresolved core is largely due to the SNRs and hot bubbles of the central starburst. Near-IR spectroscopy of the nucleus (Krabbe, Sternberg & Genzel 1994) favours a relatively young starburst (age ~ 50 Myr with a star formation rate of ~ 1 M$_\odot$ yr^{-1}); see §4.1). But at higher energies, there is evidence for a heavily obscured AGN component (q.v. Jiménez-Bailón *et al.* (2005)). Thus, we retain the Seyfert 2 classification in Table 2 for this galaxy, although the designation remains uncertain.

Figs. 8−10 present the new SPIRAL observations. NGC 1808 was observed under less than ideal conditions, with variable seeing and intermittent cloud cover. But we were able to extract useful IDDs for the inner extent of the wind. Our observations reproduce the asymmetric line profiles of Phillips (1993), with blue and red shoulders corresponding to the near side outflow and counter flow, as previously reported. Due to the weakness of [O III] and [O I], the IDDs do not provide an unambiguous answer for the nature of the ionizing source in the extended filaments. But we stress that the base of the wind is enhanced in [N II]/Hα, similar to what is observed

in NGC 1482, and the line profiles are somewhat broadened. These observations are consistent with large-scale shocks in the outflowing gas.

NGC 3628

Fabbiano, Heckman & Keel (1990) presented the first strong evidence from x-ray and Hα observations for a collimated outflow suspected from earlier kinematic work (Schmelz, Baan & Haschick 1987a,b). Subsequently, a corresponding molecular disk-halo outflow was reported by Irwin & Sofue (1996). IR (Rice *et al.* 1988) and radio (Condon *et al.* 1982) measurements place this object on the well known far-IR vs. radio correlation indicating that the central energetics are dominated by star formation. At x-ray energies, no evidence is found for an active nucleus at the current detection limits (Flohic *et al.* 2006).

Observations of NGC 3628 were undertaken in less than ideal observing conditions. We were able to extract useful spectral diagnostic information from the red data, but only limited information from the blue data. Emission line maps were extracted for Hα, [N II] and [S II] and are presented in Figs. 11 & 12. The strongest line emission originates in a series of compact regions to the south-east of the SPIRAL mosaic, which we interpret as HII regions. The [N II]/Hα ratio image (Fig. 12) reveals the filamentary emission above the plane of the disk reported by Fabbiano, Heckman & Keel (1990).

The line ratios in this region show enhanced [N II]/Hα similar to what is observed in most of our starburst wind sources. Strong [O III]/Hβ is ruled out by the blue data even with its compromised sensitivity. The base of the wind is enhanced in [N II]/Hα, reminiscent of what is observed in NGC 1482, and the line profiles are somewhat broader than line emission from neighbouring HII regions. Once again, these observations are consistent with large-scale shocks in the outflowing gas.

NGC 6810

The historic classification of this object as a Seyfert 2 galaxy is based primarily on the width of emission lines in low spatial resolution spectra of the nuclear region. Coccato *et al.* (2004) noted "a higher than expected minor axis velocity dispersion and unusual kinematics" in long slit spectroscopy. Strickland (2007) concluded that NGC 6810 is in fact a "full disk" superwind galaxy and that the previous classification is based largely on misidentification of counterparts in a low resolution radio survey and the merged line profiles of an outflowing wind. This is compatible with the earlier observation (Forbes & Norris 1998) that the radio, FIR and [Fe II] properties of the inner disk are consistent with star formation. Our new SPIRAL observations (Figs. 13−15) are consistent with this interpretation. There is no evidence for AGN activity in the optical spectra, with narrow lines consistent with solar-metallicity star formation across the stellar disk. Star formation across the disk of the galaxy dominates the IDDs.

The [O III]/Hα line ratio map (Fig. 14) shows striking evidence for an "ionisation cone" on the near side of the disk. These structures are not unique to AGN sources (e.g. Pogge 1987; Tadhunter & Tsvetanov 1989)

having been observed in starburst galaxies (e.g. Shopbell & Bland-Hawthorn 1998). Leaked radiation from a starburst or an AGN, or even shocks excited by a conic outflow, can produce ionisation cones along the minor axis. In support of this statement, the [O III]/Hβ ratio in this region is characteristically low (cf. Shull & McKee (1979)). In the line ratio map, we have used Hα in place of Hβ because the stronger Hα signal reveals the cone more clearly.

Unfortunately, the weakness of [O III] emission above the galactic disk makes it difficult to unambiguously classify the excitation mechanism for the outflow gas from the IDD (Fig. 15). But we stress that the base of the wind is enhanced in [N II]/Hα similar to what is observed in NGC 1482. The high [N II]/Hα gas delineates the boundary of a chimney structure emanating from the central starburst region. The base of the chimney extends $\sim$1.5 kpc across the inner galaxy. An inspection of emission-line profiles in regions of enhanced [N II]/Hα reveals multi-component line profiles indicative of high velocity material in a blueshifted outflow on the eastern side of the disk, with the corresponding counter flow redshifted (and dust attenuated) on the opposite side. In summary, our observations provide further evidence that the off-nuclear emission in NGC 6810 is due to a large-scale galactic wind. Like NGC 1482, the dominant source of ionisation is most likely due to shock excitation of filaments entrained in the wind.

3.2. AGN

NGC 1365

Optical spectroscopy of this well known Seyfert (Veron, Lindblad, Zuiderwijk *et al.* 1980; Edmunds & Pagel 1982) reveals a broad component to the Hα line and line ratios indicative of AGN activity. Further evidence for the AGN comes from x-ray variability of the highly obscured nucleus (Ward *et al.* 1978). But based on an analysis of the radio and x-ray structure of the central regions, Stevens, Forbes & Norris (1999) suggest that the energetics are dominated by star formation, and that "the evidence of a jet emanating from the nucleus is at best marginal" (cf. Sandqvist, Jöersäeter & Lindblad (1995)). The radio/far-IR ratio is also indicative of a dominant circumnuclear starburst (Forbes & Norris 1998).

The extended ionised gas in NGC 1365 has been extensively studied with long-slit spectroscopy. On the basis of these observations, Hjelm & Lindblad (1996) propose a physical structure (wide angle, hollow conic outflow) to explain the unusual velocity structures previously reported (Phillips *et al.* 1983; Jöersäeter *et al.* 1984) in the context of an outflow (first suggested by Burbidge & Burbidge (1960)), while Storchi-Bergmann & Bonatto (1991) present clear evidence of an [O III] "ionisation cone" to the south east of the nucleus, above the plane of the disk.

The new SPIRAL observations for NGC 1365 are presented in Figs. 16−18. The reconstructed continuum image reproduces the central disk structure seen in the *HST* imaging from Fig. 1. The Hα integrated flux map suggests strong star formation in the nuclear zone, with a number of probable compact HII regions or star clusters.

Strong [O III] emission is seen to extend eastwards from the nuclear region above the plane of the disk, while a counterpart emission region seen below the disk is at lower intensity, presumably due to dust attenuation on crossing the plane of the nuclear disk. [N II] emission exhibits the classic limb-brightened arms of a conic structure to the west but such a feature is less obvious on the near side of the disk, possibly due to confusion with disk emission. Phillips *et al.* (1983) report the "remarkable kinematics of the ionised gas in the nucleus of NGC 1365" and line splitting to be most prominent in the south-eastern region, particularly in the [O III] line, observations supported by the SPIRAL data. Line splitting is evident but not complete at the resolution of the SPIRAL observations, suggesting a narrow opening angle or low velocities for the outflow.

The emission-line ratio maps shown in Fig. 17 are revealing. The counter fan of [O III] emission is evident to the west in the [O III]/Hα ratio, while the enhanced [N II]/Hα ratio usually observed in outflowing emission line gas is seen to fill the region bounded by the limb brightened [N II] structure of the western region of Fig. 16. The expected counter-flow region is visible to the east as high [N II]/Hα gas once far enough above the disk to avoid contamination by the strong star formation in the region. The [S II] electron density diagnostic shows no clear structure at the limit of our signal-to-noise limit. The ionisation cone from the central AGN is most evident on the nearside of the disk in the [O III]/[O I] ratio (Fig. 17).

The classic IDDs are presented in Fig. 18: the dominant signature is that of a high metallicity starburst consistent with dominant circumnuclear star formation. However, significant emission, particularly in the outflow regions, lies above the *extreme star formation* boundary of Kewley *et al.* (2001). The zone occupied by this gas, in all three of the classic diagnostic diagrams, is indicative of the hard ionising spectrum expected from AGN photoionisation, and is for the most part inconsistent with photoionisation by starlight or shock ionisation models. Broad HeII λ4686 and HeI λ5876 emission are observed in the nuclear spectrum, consistent with photoionisation by a hard ionizing source.

CIRCINUS

Located at low galactic latitude and with high foreground extinction (A$_V$=1.5), this large nearby Seyfert galaxy was first identified by Freeman *et al.* (1977). Maser measurements firmly establish the central black hole mass at $m_{\mathrm{BH}} \approx 2 \times 10^6$ M$_\odot$ (Greenhill *et al.* 2003a). With the inferred accretion rate ($\approx$0.1 L_{edd}) at odds with much higher accretion rates in other Seyferts with maser-determined black hole masses (e.g. NGC 1068; Begelman & Bland-Hawthorn 1997), Circinus lends support to the notion that supermassive black holes are indeed quite common in galaxies, but for the most part have long duty cycles and/or low accretion rates.

The Seyfert 2 nature of Circinus is supported by the mid-IR coronal line emission (Lutz *et al.* 2002), e.g. [Si IX] at 3.94μm (Oliva *et al.* 1994). Recent integral field spectroscopy, assisted by adaptive optics (Mueller-Sánchez, Davies, Eisenhauer *et al.* 2006), indicates a substantial (1−2% L_{bol}) young (<100 Myr) toroidal starburst within 10 pc of the central AGN and provides further evidence for a "wide angle outflow" as reported

by Greenhill *et al.* (2003b). Extended filamentation associated with the outflow was first mapped by Veilleux & Bland-Hawthorn (1997), and later in more detail by Veilleux *et al.* (2003). X-ray spectral analysis further supports the view of Circinus as a highly obscured AGN but with strong thermal dust emission dominated by heating from nuclear star formation (Matt *et al.* 2000).

The large spatial extent of the Circinus galaxy allowed only the north-west side of the disk to be probed with SPIRAL. Figs. 19−21 present the observations. Our spatial coverage was guided by *TTF* observations of Veilleux & Bland-Hawthorn (1997) and the *HST* study of Wilson, Shopbell, Simpson (2000). We have not attempted to correct the observed spectra for foreground reddening. The "hook" structure identified by Veilleux & Bland-Hawthorn (1997) traces the southern boundary of an ionisation cone, running east-west in the prominent emission lines.

The [O III] line profiles show significant complexity with a number of mixed velocity components. Maximal line splitting in the centre of the ionisation cone, and single line profiles along its outer walls, might suggest a simple conic outflow structure. But the line intensity maps indicate limb darkening rather than the limb brightening one would expect on a conic emitting surface at the interface of a hot wind material and the cooler ISM, suggesting significant emission from gas within the cone. There is a strong velocity gradient across the filaments, each filament being at a different mean velocity, with the [O III] emission from the east-west boundary significantly redshifted with respect to the opposite (north-south) region of the ionisation cone. The ouflow is best interpreted as a gas-filled ionisation cone illuminated by the central AGN, rather than a walled cavity structure.

NGC 5128 (CENTAURUS A)

Cen A is one of the most well studied active galaxies owing to its extraordinary brightness across 16 decades or more of the electromagnetic spectrum (Israel 1990). It is the nearest powerful AGN and, more specifically, the closest FR I radio source. Fortuitously, we are witnessing an accretion-powered radio source in the first 100 Myr of its projected $0.5 − 1$ Gyr lifetime. A well known feature of Cen A, unique among our sample, is the presence of a spectacular radio jet (Blanco, Graham, Lasker & Osmer 1975; Peterson, Dickens & Cannon 1975) which ignites optical filaments along its axis (Sutherland, Bicknell & Dopita 1993). The jet-induced emission falls far beyond the radial extent of our IFU mosaic.

Over the inner galaxy, the extended ionised gas was first mapped by Bland, Taylor & Atherton (1987) and Nicholson, Bland-Hawthorn & Taylor (1992), and shown to arise exclusively from a severely-warped thin disk, later confirmed by CO observations (Quillen, Graham & Frogel 1993). A diffuse highly ionised halo of [O III] was first identified by Bland-Hawthorn & Kedziora-Chudczer (2003, see their Fig. 6) and has recently been shown to match the extended x-ray maps from *Chandra* (Kraft *et al.* 2008) extraordinarily closely. Extended mid-IR emission is also seen along the radio axis, revealing evidence for a limb-brightened shell (Quillen *et al.* 2006), and providing strong evidence for a bipolar outflow along the radio axis.

Here we provide only a brief summary of the SPIRAL observations presented in Figs. 22−24. A more detailed discussion and associated modeling is to be presented elsewhere. The [O III]/Hβ vs. [N II]/Hα IDD reveals a large number of data points above the extreme starburst line. When these points are identified in the SPIRAL data, they reveal a striking nuclear ionisation cone. The cones vissibility is enhanced after a 3×3 spatial binning of the mosaiced blue IFU data (Fig. 25). The conic region, delineated by sharp edges, exhibits gas with the ionisation ratios expected from a hard AGN ionising spectrum, although shocks cannot be ruled out. The structure can be traced back towards the nucleus where it likely connects with the Paβ emission cone seen by Krajnović, Sharp & Thatte (2007) at near-IR wavelengths. The feature is roughly aligned with the known radio jet structure above the plane of the disk. Our coverage to the south is insufficient to trace a possible counter cone. Throughout the cone, we clearly see variations in the [S II] doublet consistent with density variations of order $n_e \approx 300 − 1000$ cm^{-3}. This is consistent with the inferred shell-enhanced densities from the mid-IR observations (Quillen *et al.* 2006).

In summary, we have discovered an "ionisation cone" along the minor axis of Centaurus A for the first time. The phenomenon is most evident in emission-line ratio images (e.g. [O III]/Hβ) where a clear distinction can be made between the ionising source in the outflow from the background ionising source. This tends to favour an ionisation cone powered by an AGN source, but the phenomenon can also be identified in starburst galaxies (see §4.1), as we discovered here in NGC 6810.

IC 5063

Bergeron, Durret & Boksenberg (1983) presented early evidence for an obscured Seyfert nucleus via the detection of a broad yet weak component to the Hα emission. Colina, Sparks & Macchetto (1991) reported high-excitation emission lines and confirmed the broad Hα profile, thereby supporting the claim of a concealed active nucleus. Both papers note the kinematic decoupling of gas in the inner regions from the extended disk rotation curve of the galaxy. Colina, Sparks & Macchetto (1991) favoured an explanation invoking outflowing gas, and provided evidence of a wide angle (50°) ionisation cone via the spatial map of the [O III]/Hα ratio.

At radio wavelengths, Morganti *et al.* (2007) present high quality observations of warm and cool material moving outwards from the nucleus (see also Morganti, Oosterloo & Tsvetanov (1998)). Their observations suggest a radio lobe/jet structure which in turn may be responsible for the disturbed kinematics of the outflow gas. These authors conclude there is little evidence for shock-driven excitation, proposing instead that the emission is overwhelmed by AGN photoionisation.

The SPIRAL observations are shown in Figs. 26−28. As presented in previous work (Bergeron, Durret & Boksenberg 1983; Colina, Sparks & Macchetto 1991), the velocity field of the emission line gas is dominated by a regular disk rotation beyond $2''$ from the nucleus, although line profiles show evidence of broadening at the base of the stronger lines, and line splitting is apparent above the mid-plane. The kinematically distinct outflow-

ing gas shows little evidence of the classic line splitting expected from a hollow conic outflow structure, indicative of a more homogeneous gas distribution in this region. The ionisation diagnostic diagrams (Fig. 28) indicate AGN photoionisation almost exclusively, at least in regions where the intensity of emission is sufficently above the fitting threshold.

NGC 6240

As one of the closest of the ultraluminous infrared galaxies (ULIRG), NGC 6240 is central to the longstanding debate as to the presence or absence of quasar-like nuclei in ULIRG sources. In the case of NGC 6240, hard x-ray observations unambiguously identify a double AGN core at its heart (Komossa *et al.* 2003). A large-scale wind was first reported by Heckman, Armus and Miley (1990) (cf. Ptak, Heckman, Levenson *et al.* (2003), Colbert, Wilson & Bland-Hawthorn (1994)). The extended emission-line gas has been mapped in optical lines by imaging tunable filters (Bland-Hawthorn, Wilson & Tully 1991; Veilleux *et al.* 2003) and in x-ray emission (Komossa *et al.* 2003).

The SPIRAL observations show that the nuclear regions of NGC 6240 are highly complex both in the kinematics and ionised gas distribution. With limited spatial coverage possible due to observing constraints, our observations were guided by the study of Veilleux *et al.* (2003) and focus on the region of high [N II]/Hα ratio emission. Two dimensional emission maps are not shown as the complexity of the emission structure in the nuclear region combined with the low surface brightness of emission in the less complex outer zones is not easily interpreted in this manner. Spectra from the nucleus show kinematically broadened line emission (FWHM$\sim$13Å) with a velocity spread of 500-600 km s^{-1}. Most spectra do not easily separate into identifiable Hα and [N II] lines.

An emission-line filament is observed to extend east from the nucleus. We interpret the isolated line in the filament spectrum as Hα offset in velocity from the host galaxy by +340 km s^{-1} in the outer reaches of the mosaic. This is at odds with the Hα vs. [N II] map of Veilleux *et al.* (2003) but we note that the proposed shift in the emission wavelength could lead to cross-contamination between the wavelength settings of the tunable filter observations. The conspicuous absence of satellite Hα (and the fainter [N II] line) in the filament spectrum support our proposed identification. On heavily binning adjacent spectra, there is evidence for a weak feature compatible with broad [N II] emission to accompany Hα. There is tentative evidence for [O III] emission associated with the Hα filament as well, although the sensitivity of the data is not sufficient to confirm this in detail. In summary, we are unable to construct IDDs for this object with the present observations.

4. AGN VS. STARBURST

In the previous section, we saw consistent differences in the ionisation characteristics of outflowing gas associated with starburst and AGN sources. We now present a simple model that largely explains these differences. Consequently, our model provides a key insight into the galactic wind mechanism and the radiative timescales of the starburst and AGN phenomenon.

4.1. *Predicted and observed levels of photoionisation*

Our galaxy sample spans bolometric luminosities in the range $L_{\rm bol} = 1 - 10 \times 10^{10}$ L$_\odot$ and are distinguished by their nuclear starburst or AGN activity. All of the galaxies were selected on the basis of known minor-axis outflows. The new observations reveal that all of the AGN galaxies display IDDs typical of direct photoionisation by the AGN, whereas the starburst galaxies display IDDs typical of shock ionisation. How are we to understand this?

First we note that both nuclear starburst and active galaxies almost certainly have duty cycles such that what we observe now is more representative of their peak activity rather than their quiescent phase. We now show that *prima facie* the distinction between starburst and AGN outflow IDDs is surprising when one considers the overall ionizing photon production in both classes of sources.

A black hole that converts rest-mass energy with an efficiency ϵ into radiation has a luminosity

$$L_A = \epsilon \dot{m} c^2 \tag{1}$$

$$= 7 \times 10^{11} \left(\frac{\epsilon}{0.05} \right) \left(\frac{\dot{m}}{M_\odot \ {\rm yr}^{-1}} \right) \ L_\odot \tag{2}$$

for which $\dot{m}$ is the mass accretion rate. In reality, the accretion disk luminosity can limit the accretion rate through radiation pressure. The so-called Eddington limit is given by

$$L_E = \frac{4\pi G m_{\rm BH} m_p c}{\sigma_T} \tag{3}$$

$$= 2 \times 10^{11} \left(\frac{m_{\rm BH}}{10^7 \ M_\odot} \right) \ L_\odot \tag{4}$$

where $m_{\rm BH}$ is the black-hole mass, m_p is the proton mass and σ_T is the Thomson cross-section for electron scattering. This equation allows us to derive a maximum accretion rate $\dot{m}$, and therefore a maximum ionizing luminosity, for a given black-hole mass. We find that this relation is not strongly constrained with the present data. For a canonical power-law continuum ($\propto (h\nu)^{-1}$) typical of active galactic nuclei, the number of Lyman continuum (LyC) photons is given by

$$\mathcal{N}_{\rm LyC,A} \sim 10^{54} \xi_A \left(\frac{L_{\rm bol,A}}{10^{11} L_\odot} \right) \ {\rm phot \ s}^{-1} \tag{5}$$

for which ξ_A is the fraction of $L_{\rm bol}$ ($L_A = \xi_A L_{\rm bol}$) arising from AGN activity today (i.e. not averaged over the lifetime of the source).

The total radiative output from a luminous starburst at the present epoch can be approximated by (e.g. Maloney 1999; Heckman, Lehnert & Armus 1993)

$$L_S \sim 10^{11} \left(\frac{\dot{s}}{5 \ M_\odot \ {\rm yr}^{-1}} \right) \left(\frac{\Delta t}{10^8 \ {\rm yr}} \right)^{0.67} \tag{6}$$

$$\times \left(\frac{m_L}{1 \ M_\odot} \right)^{0.23} \left(\frac{m_U}{100 \ M_\odot} \right)^{0.37} \ L_\odot \tag{7}$$

where Δt is the starburst duration estimated from the gas supply divided by the star formation rate $\dot{s}$. The third and fourth terms indicate the lower and upper stellar mass cut-offs. For a conventional IMF, the star for-

mation rate is roughly

$$\dot{s} \sim 5 \left(\frac{L_S}{10^{11} \, L_\odot} \right) \left(\frac{\Delta t}{10^8 \, \text{yr}} \right)^{-0.67} M_\odot \, \text{yr}^{-1}. \quad (8)$$

We can now determine the rate of Lyman continuum photons produced by the starburst. To a useful approximation,

$$\mathcal{N}_{\text{LyC,S}} \sim 10^{54} \left(\frac{\dot{s}}{5 \, M_\odot \, \text{yr}^{-1}} \right) \left(\frac{m_L}{1 \, M_\odot} \right)^{0.23} \left(\frac{m_U}{100 \, M_\odot} \right)^{0.37} (9)$$

$$\sim 10^{54} \xi_S \left(\frac{L_{\text{bol}}}{10^{11} L_\odot} \right) \text{ phot s}^{-1} \qquad (10)$$

which is to be compared to equation 5 above. The high-energy cut-off for the hot young stars declines rapidly beyond 50 eV. The factor ξ_S is the fraction of L_{bol} ($L_S = \xi_S L_{\text{bol}}$) arising from the starburst activity today (i.e. not averaged over the lifetime of the source).

The LyC photon rate for both starbursts and AGNs for two sources with the same bolometric luminosity is essentially the same. While the nonthermal spectrum of the AGN means that the harder photons propagate at least an order of magnitude further into the surrounding gas, the photon *number* is dominated by the soft photons so that the comparison is still meaningful. We do not discuss the possibility of the *total* accretion disk luminosity being channelled into a smaller solid angle (i.e. intrinsically beamed) because we were unable to find compelling evidence for this to be so. This is to be addressed in our later papers.

An ionizing photon rate as high as $\mathcal{N}_{\text{LyC}} \sim 10^{54} \xi$ $(L_{\text{bol}}/10^{11} L_\odot)$ phot s^{-1} is easily large enough to account for the off-nuclear line fluxes observed in all galaxies, whether starburst or AGN. At a distance of 1 kpc, the ionizing flux is $\varphi \approx 10^{10}$ phot cm^{-2} s^{-1}. We can relate this to the Hα surface brightness through the emission measure $\mathcal{E}_m$ where

$$\mathcal{E}_m = \int f n_e^2 \, \text{d}z \quad \text{cm}^{-6} \, \text{pc} \qquad (11)$$

which is an integral of H recombinations along the line of sight z multiplied by a filling factor f.[5] If we assume that the absorbing cloud along the minor axis is optically thick, we can relate this directly to an Hα surface brightness in cgs units such that

$$\mu(\text{H}\alpha) = 1 \times 10^{-14} \left(\frac{r}{1 \, \text{kpc}} \right)^{-2} \left(\frac{L_{\text{bol}}}{10^{11} L_\odot} \right) \quad \text{cgs} \quad (12)$$

where r is the distance to the central source (Bland-Hawthorn *et al.* 1998, Appendix). Therefore the expected Hα surface brightness at 1 kpc is roughly 7×10^{-15} cgs for the AGNs, and 2×10^{-15} cgs for the starbursts. (The difference here relates to the different mean bolometric luminosities between the two classes of objects.) These predictions are an order of magnitude brighter than what is seen in our objects (Table 4), with the possible exception of the AGN IC 5063 where the minor axis filaments are very bright. The higher predicted values may be due

---

[5] $\mathcal{E}_m(\text{H}\alpha) = 1$ cm^{-6} pc is equivalent to 2×10^{-18} erg cm^{-2} s^{-1} arcsec^{-2} (cgs) for a plasma at 10^4 K.

to a combination of several factors: (i) the emitting regions have a small filling factor ($f < 1$), (ii) some dust is mixed in with the filaments (cf. Cecil *et al.* 2001), and (iii) $\xi < 1$ for the AGN/starburst fraction of the bolometric luminosity.

Thus we find that both AGNs and starbursts have the capability to ionise much of the extended gas filaments observed far along the minor axis, assuming that the radiation is not scattered or absorbed en route. So we arrive at an important conclusion. *The distinction between starburst and AGN outflow IDDs is one of timescale*, assuming that the wind mechanism is not too dissimilar between the two sources (e.g. Veilleux *et al.* 2005). The time evolution of UV photon production must be radically different in both cases. To explore this issue further, we examine more closely how the energy is deposited into the surrounding medium.

4.2. *Time evolution of UV and mechanical luminosity in a starburst*

The starburst phase in a galaxy's life is a spectacular phenomenon that can be observed to very high redshifts. Just how the formation of hundreds of millions of stars can be triggered over the central regions of galaxies in a dynamical time remains an open issue. What is well known is that the high mass stars evolve rapidly, giving off prodigious amounts of UV radiation initially before entering into the supernova phase, whereupon a huge amount of mechanical energy is deposited into the ISM (Leitherer *et al.* 1992).

In Fig. 29, we show the results from running *Starburst99* with a conventional initial mass function (IMF) for both instantaneous and continuous star formation models. We show the time evolution of the ionizing and mechanical luminosities arising from the starburst. Two upper mass cut-offs are presented in order to illustrate the important contribution of the highest mass stars. In Fig. 29(a), the rapid drop in UV production at 10 Myr is evident, as is the rise of mechanical output from supernovae beyond here. This corresponds to stars more massive than $13 M_\odot$ evolving off the main sequence to become supernovae.

Fig. 29(a) can readily account for why stellar photoionisation does not dominate over shock ionisation. Thus, we conclude that the ionisation timescale (T_I) indicated by starburst winds is such that $T_I \gtrsim 10$ Myr. Fig. 29(b) effectively rules out the continuous star formation model, at least for the starbursts in our sample. The model predicts that stellar photoionisation is detectable at all times contrary to what we observe.

In the next section, we show that the predicted mechanical luminosity in the instantaneous star formation model is more than enough to explain the observed shock ionisation. Indeed, we argue that Fig. 29 dates the observed starburst wind phenomenon in the range 10 to 40 Myr. A more precise age will depend on how the starburst region evolved early in its life (Suchkov *et al.* 1994; Cooper *et al.* 2008). We discuss this issue in more detail below.

4.3. *Time evolution of UV and mechanical luminosity in an AGN*

We must now explain the dominance of AGN photoionisation of the filaments in AGN wind objects. There

are few reliable constraints on the long-term temporal evolution of accretion-disk radiation fields. Like starbursts, AGNs clearly display all the hallmarks of duty cycles, bursts and outflows over the course of their lifetimes (Soltan 1983; Cavaliere & Padovani 1990). Most galaxies appear to have central massive black holes, but only a few percent can be classified as AGNs. The most likely explanation is that almost any galaxy can display AGN activity if its nuclear regions experience substantial gas accretion from outside.

But we arrive at the long-standing debate on what can be uniquely attributed to the AGN as compared to, say, circumnuclear star-forming activity (Terlevich *et al.* 1985). After all, the gas inflow that triggers the former can just as easily give rise to the latter. These activities are commonly seen in close proximity, in particular, in Seyfert galaxies. We address both of these issues now, i.e. why the AGN dominates the photoionisation of the wind filaments, and whether our conclusions are affected by the presence of the circumnuclear starburst.

A reasonable AGN scenario is that the activity is initially triggered by a gas dump, followed by a slow decline in the fuelling process (e.g. Norman & Silk 1983) as the gas settles down within the nuclear potential well. We assume an exponential model for the UV output from an AGN such that

$$L_A/L_{\rm bol} = C_{\rm A,max} \exp(-t/t_A) \qquad (13)$$

where $C_{\rm A,max}$ is the maximum fraction of the bolometric luminosity that the AGN achieves over the lifetime of the activity with half life t_A. We further restrict this relation using the following normalization:

$$\int_{\rm LL}^{\infty} \frac{L_A}{h\nu} \, d\nu = \mathcal{N}_{\rm LyC,A} \qquad (14)$$

where LL denotes the Lyman limit ($h\nu = 13.6$ eV) and the RHS is given by equation 5. In practice, this normalization for $C_{\rm A,max}$ and t_A is difficult to do properly because our observations constitute an instantaneous snapshot, rather than the time-averaged behavior of its properties. Of course, the same holds true for starburst activity. In principle, IFU studies of a large sample of AGNs and starbursts could provide accurate measurements of ξ_A and ξ_S and therefore provide strong constraints on $C_{\rm max}$ for both AGNs and starbursts.

If we integrate equation 13 over time ($\Delta t = 100$ Myr), subject to the normalization in equation 14, we arrive at the important result that $C_{\rm A,max} \propto t_A^{-1}$. The normalization ensures that a range of AGN models depending on $C_{\rm A,max}$ and t_A produce the same ionizing radiation field averaged over the lifetime of the source. In Fig. 30, we superimpose four such models on the instantaneous starburst model in Fig. 29.

As already mentioned, essentially all of our AGN sources show appreciable circumnuclear star formation. Since AGN photoionisation is clearly dominant over stellar photoionisation in all of our AGN sources, the predicted surface brightness values effectively rule out AGN exponential timescales below 10 Myr. If the AGN UV radiation field is "beamed" along the wind axis, in the sense that the AGN source is *strongly* anisotropic, then shorter AGN timescales are possible. But the dynamical timescale of the wind discussed in the next section argues

against this interpretation. Furthermore, we have been unable to find any reliable evidence for a UV boost along the wind axis in AGNs.

But a question remains. In Fig. 30, note how the starburst mechanical luminosity can dominate over the AGN UV luminosity beyond 10 Myr, assuming the mass/energy input can be efficiently converted to ionizing radiation. Why do we therefore not see the signatures of shocks in AGN-driven winds? Shocks are seen in *starburst* winds because the central ionizing source fades rapidly early in the evolution of the wind. But this problem only arises if we assume that the mechanical energy in the AGN sources is supplied with a long delay as for starburst-driven winds because, for example, the AGN wind is assisted by a circumnuclear starburst. The observations may therefore indicate that the AGN-driven winds are fundamentally different from starburst-driven winds. In this scenario, the mechanical energy is supplied by the accretion disk immediately, but the shock ionizing luminosity never exceeds the luminosity of the central accretion disk.

We now consider the shock ionisation observed in starburst-driven winds. We find that only a fraction of the available mechanical luminosity must be used in shock-exciting the gas, either because the process is inefficient or because the filling factor of the extended filaments is lower than unity.

4.4. *Dynamical timescale of a large-scale wind*

Here we address the dynamical timescale of galactic winds before going onto derive levels of optical emission powered by shock ionisation. Once the starburst or AGN fires up, it begins to deposit energy into its surroundings. This largely mechanical energy over-pressurizes a circumnuclear cavity of hot gas that reaches a temperature

$$T \approx 3 \times 10^8 \; \chi \; \Lambda^{-1} \; \text{K}, \qquad (15)$$

where χ is the efficiency of turning mechanical energy into heat, and Λ is the mass-loading factor (Veilleux *et al.* 2005). This ratio measures the total mass of heated gas to the mass that is directly ejected by SNe and stellar winds or by the AGN. Most galactic winds appear to entrain gas from the interstellar medium as shown by the rotation of this material about the flow axis (see Veilleux *et al.* (2005) for a detailed discussion). The entrained gas, which can easily dominate the wind mass, is accounted for with Λ typically larger than unity (e.g. Suchkov *et al.* 1994).

The central cavity is too hot to cool efficiently and so builds up a pressure

$$P_o/k \sim 2 \times 10^6 \; \left(\frac{\dot{s}}{5 \; M_\odot \; {\rm yr}^{-1}} \right) \left(\frac{R_*}{1 \; {\rm kpc}} \right)^{-2} \; {\rm K \; cm}^{-3}$$

$$(16)$$

where R_* is the radius of the energy injection zone. This pressure can significantly exceed the pressure of the undisturbed ISM. The hot cavity then evolves like a stellar wind-blown bubble (e.g., Castor, McCray, & Weaver 1975; Koo & McKee 1992a,b). As hot gas expands through the sonic radius, it cools adiabatically. Beyond the sonic radius, the wind drives a shock into the surrounding ISM and starts to sweep up a shell of shocked gas, a process that gradually slows the bubble

to much less than the wind velocity. This marks the end of the adiabatic "free expansion" phase, whose duration is set by the mechanical luminosity of the starburst or AGN and the original density of the ISM. After free expansion, the system develops distinct concentric zones from the centre moving outwards due to the strong shocks (Cooper et al 2008; Dopita & Sutherland 1996; Weaver et al. 1977).

Energy-conserving bubbles. If radiative losses of the overall system are negligible, the expanding bubble is energy-conserving. In that case, the radius and the velocity of the expanding shell of shocked ISM are given by (Castor et al. 1975; Weaver et al. 1977)

$$r_{\text{shell}} = 1.1 \ (\dot{E}_{44}/n_o)^{1/5} \ t_6^{3/5} \ \text{ kpc}, \qquad (17)$$

and therefore

$$V_{\text{shell}} = 640 \ (\dot{E}_{44}/n_o)^{1/5} \ t_6^{-2/5} \qquad (18)$$

$$= 670 \ (\dot{E}_{44}/n_o)^{1/3} \ r_{\text{shell,kpc}}^{-2/3} \ \text{ km s}^{-1} \qquad (19)$$

where t_6 is the age of the bubble in Myr, n_o is the ambient density in cm^{-3}. By convention, we use $\dot{E}_{44}$ for the mechanical luminosity of the wind in units of 10^{44} erg s^{-1} ($\dot{E}_{44} \approx \xi L_{\text{bol}}/4 \times 10^{11} L_\odot$).

Momentum-conserving bubbles. If radiative losses are significant, momentum conserving bubbles decelerate somewhat faster such that $r_{\text{shell}} \propto t^{\frac{1}{2}}; V_{\text{shell}} \propto t^{-\frac{1}{2}} \propto r_{\text{shell}}^{-1}$ (e.g., Avedisova 1972; Steigman, Strittmatter, & Williams 1975; Koo & McKee 1992a,b). For the galaxies we are considering here, the inferred timescales are roughly comparable (see Table 5).

TABLE 5
A COMPARISON OF EXPANSION TIME (t_6 IN MYR) AND SHELL VELOCITY (V_{shell} IN KM S^{-1}) FOR A BUBBLE THAT HAS EXPANDED TO A RADIUS r_{shell} (IN KPC). VALUES ARE SHOWN FOR AN ENERGY CONSERVING AND A MOMENTUM CONSERVING BUBBLE.

r_{shell}	energy conserving		momentum conserving	
	t_6	V_{shell}	t_6	V_{shell}
1	0.6	871	0.5	871
2	1.7	549	2.0	616
3	3.4	419	4.4	503
4	5.6	346	7.8	435
5	8.1	298	12.2	390

In most simulations to date, the terminal velocity of gas entrained by a galactic wind is $V_t \sim 400 - 800$ km s^{-1} (e.g. Suchkov et al. 1994; Cooper et al. 2008). Proper comparisons are difficult because the models deal with clumpiness in the entrained gas, which the scaling relations above do not. Chevalier & Clegg (1985) provide a useful formula for the terminal velocity of a cloud accelerated by a wind (see also Strickland & Heckman 2008):

$$V_t \approx 430 \ f_e^{1/4} f_m^{1/4} (r_o/1 \text{ kpc})^{-1/2} (\sigma_o/10^{-3} \text{g cm}^{-2})^{-1/2} \qquad (20)$$

where r_o and σ_o are the initial distance and column density of the cloud. (This formula is specific to the "constant velocity" phase of the wind before it breaks free of the confining medium.) The factors f_e and f_m account

for the fractions of supernova energy and mass respectively that work to heat the diffuse gas. These authors explore fractions in the range 0.1 to 1 and ultimately favour the high end of this range. In any event, the dynamical time of the wind is roughly $\tau_D \geq r_o/V_t \sim 2$ Myr (see also Cooper et al. 2008) which is considerably longer than the cooling time of the entrained gas.

The wind timescale is comparable to the dynamical time of the starburst region itself, but is up to an order of magnitude less than the ionisation timescale T_I established by our analysis above. This is a striking result that suggests a substantial delay ($\gtrsim 10$ Myr) after the onset of star formation before the conditions for a large-scale wind are properly established.

4.5. *Shock ionisation in a large-scale wind*

In the starburst wind objects, the overall ionisation properties are consistent with shock processes (see §3.1). A simple calculation can validate this. From Dopita & Sutherland (1996), the total shock luminosity is

$$L_{\text{shock}} \approx 2 \times 10^{34} V_{\text{shock}}^3 n_o A_{\text{shock}} \ \text{ erg s}^{-1}. \qquad (21)$$

These authors find that about 50% of the mechanical energy is converted into energy capable of ionizing gas. Assuming there is sufficient gas to soak up the ionizing photons, one can derive a useful relation for the Hα luminosity, such that

$$L_{\text{shock}}(\text{H}\alpha) \approx 0.01 L_{\text{shock}} V_{\text{shock}}^{-0.6} \ \text{ erg s}^{-1}. \qquad (22)$$

We now derive a canonical Hα surface brightness for shock-ionised filaments associated with the galactic wind. For a galaxy at a distance of $D = 10$ Mpc, the observed Hα flux from the shock is

$$f_{\text{shock}}(\text{H}\alpha) \approx 2.4 \times 10^{-20} V_{\text{shock}}^{2.4} n_o A_{\text{shock}} \left(\frac{D}{10 \text{ Mpc}} \right)^{-2} \qquad (23)$$

$$\text{erg cm}^{-2} \text{ s}^{-1} \qquad (24)$$

which assumes, consistent with Dopita & Sutherland (1996), that only a single shock surface is observed with no correction for possible limb brightening.

The surface brightness of shocked emission at 1 kpc follows:

$$\mu_{\text{shock}}(\text{H}\alpha) \approx 5.2 \times 10^{-16} \left(\frac{V_{\text{shock}}}{100 \text{ km s}^{-1}} \right)^{2.4} \left(\frac{n_o}{10 \text{ cm}^{-3}} \right) \text{ cgs} \qquad (25)$$

The pre-shock density normalization assumes that the halo gas in starburst galaxies follows an isothermal distribution (e.g. Cooper et al. 2008) normalised to a pre-shock density of $n_o = 10$ cm^{-3} at 1 kpc consistent with material swept up in a wind (q.v. Chevalier & Clegg 1985; see below). Post-shock densities inferred from the [SII] doublet (e.g. McCarthy et al. 1987) are typically in the low density limit (< 100 cm^{-3}) beyond $r = 300$ pc.

While equation 25 has a strong dependence on V_{shock}, the shock speed is well constrained by observation. Some authors have associated the terminal velocity of entrained gas with the shock velocity induced by the wind (e.g. Maloney 1999). But the levels of ionisation tell a different story. The strong [NII]/[OIII] signal favours shock velocities of order 100 km s^{-1} (e.g. Shopbell & Bland-Hawthorn 1998; Veilleux & Rupke 2002). This is

supported by the soft x-ray emission which appears to be powered by similar shock velocities. How are we to understand this?

In our picture, the fast hot wind accelerates denser gas to a terminal velocity. These clouds are ram-pressure confined by the fast wind. We therefore write down a simple equation for shocks driven into the clouds such that

$$n_w(V_w - V_t)^2 = n_o V_{\text{shock}}^2 \qquad (26)$$

where n_w and V_w are the wind density and velocity.

Strickland & Heckman (2009) have recently conducted an excellent re-evaluation of Chevalier & Clegg's original model for the M82 wind. The free-flowing or break-out wind speeds can be as high as $V_w = 3000$ km s^{-1}. For our adopted values of n_o, V_{shock} and V_t above, we can balance equation 26 with $n_w \sim 0.01$ cm^{-3}, a factor of a few higher than the canonical solution at 1 kpc presented by Strickland & Heckman (2009). We consider this to be broadly consistent given the uncertainties. In our simple analysis, the shock velocity is always several times less than the terminal velocity of clouds caught in the flow.

Our simple model leads to an Hα surface brightness of $\approx 5 \times 10^{-16}$ cgs at 1 kpc. This approximate value is comparable to what is presented in Table 4 for the starburst galaxies. In principle, the filling factor of the shocked material can be low ($f < 1$), and there will be moderate levels of extinction internal to the entrained gas (i.e. $A_V < 0.3$ mag; Cecil *et al.* 2001). But in principle, a moderately fast shock could account for the observed, extended line emission.

We note that the Hα surface brightness in equation 25 is comparable to the observed AGN surface brightness in Table 4, but much fainter than the predicted AGN surface brightness in equation 12. This may indicate that the filling factor in the wind filaments is $f \approx 0.1$. Fortunately, a discussion of the *relative* merits of different ionisation sources does not require knowledge of the gas filling factor f. A lower filling factor affects the theoretical prediction identically in equations 12 and 25, and usefully brings our models into line with the observations, at least in principle. Thus, if AGN winds involve similar processes to starburst winds, we would not expect shocks to outshine direct photoionisation from the AGN, consistent with our observations.

We have already argued that shocks outshine direct stellar photoionisation from the starburst because the young starburst has dimmed tremendously by the time the wind breaks out. Close to the disk, we may still expect stellar photoionisation to dominate over shocks owing to large-scale star formation in the disk (Bland-Hawthorn & Maloney 1999). But much beyond 300 pc or so, wind-driven shocks can dominate the ionisation, as observed in our sample. If we invoke a lower filling factor consistent with AGN winds, we can readily explain NGC 3628, but now NGC 253 and NGC 1482 appear overluminous. Indeed, a careful study of Table 4 reveals the need to change f over the range (0.1,1) to match our model to all of the observations. This may indicate that our model is oversimplified and needs to include a gas filling factor, or even a correction for internal extinction (although this is found to be typically less than 10% from the SPIRAL observations in the brightest regions). We note two things: (i) the inferred filling factors are not unreasonable and can be directly measured in principle; (ii) alternatively, the inferred extinction corrections are plausible, and these can also be directly inferred from the Balmer decrement with data of sufficient sensitivity.

5. SEQUENCE OF EVENTS: THE BIRTH AND EVOLUTION OF GALACTIC WINDS

We conclude with a "big picture" model of the starburst wind phenomenon. Our purpose is to provide a physical explanation for the delay before the galactic wind gets going. We believe that this simple model explains the broadest features of our new SPIRAL observations. Therefore the stages of evolution for a galactic wind are as follows:

(1) Stars are born in dense molecular clouds whereupon the hot massive stars produce a strong UV radiation field (Lada & Lada 2003);

(2) The mean free path of Lyman continuum photons is greatly extended by stellar winds (and radiation pressure) that blow bubbles into the surrounding ISM. (Good discussions of this process are to be found in Castor *et al.* 1975; Weaver *et al.* 1977; MacLow & McCray 1988; Tomisaka & Ikeuchi 1988.) The intense UV radiation ionizes any pre-existing intracloud medium but this may have been cleared out by an earlier wind.

(3) The over-pressured warm gas evaporated from the surfaces of dense clouds helps to fill the wind-blown "voids" and intracloud region. The connection between the evaporating cloud skins and the intracloud wind material may help the wind to entrain denser gas from these same clouds (Cooper *et al.* 2008).

(4) The bulk of the supernova ejecta arises after 8-10 Myr (Fig. 29; Leitherer *et al.* 1992). As noted by others (e.g. Chevalier & Clegg 1985), the ejecta ultimately thermalizes the diffuse material which escapes as a wind; any shock heating of the denser medium escapes as infrared radiation (Strickland & Stevens 2000). The UV intensity declines dramatically since many of the high-mass stars have now exploded.

Thus we are led to an important conclusion. *The large-scale wind cannot become established until vast quantities of warm diffuse gas are dislodged from the surfaces of dense clouds by UV evaporation.* The ionised material with a sufficiently long cooling time is then mechanically heated by the supernova mass/energy input. It is therefore not surprising that, by the time the wind gets going, most of the short-lived massive stars have faded or disappeared. We would therefore *not* expect to see a strong signature of stellar photoionisation in the extended wind filaments if the starburst phenomenon arises from a *single* burst of star formation. *Our new observations may provide the strongest evidence yet that starbursts truly are impulsive events.* The fact that the signature of AGN photoionisation *is* clearly visible in the wind filaments argues that the accretion-disk UV timescale is considerably longer than the starburst timescale. Furthermore, unlike the starburst, the mechanical energy input *must* have occurred early in the life of the AGN, presumably at a time when jets can also be launched. We argue that our observations are a testament to this simple picture.

Conversely, if there are starburst sources where stellar photoionisation *does* dominate at large radial distances

(cf. Shopbell & Bland-Hawthorn 1998), we anticipate that the circumnuclear regions in these sources are characterised by an extended episode of star formation (i.e. continuous star formation) due to an extended period of fuelling and accretion (e.g. sustained merger activity).

6. SUMMARY

The role of mass/energy feedback and recycling in galactic winds over cosmic time is very poorly understood. In particular, we are far from a detailed understanding of how gas accretion to the circumnuclear regions fuels local star formation and nuclear activity. So what can we say?

The galaxy wind phenomenon is well established and its influence can be detected in the highest redshift sources (Heckman *et al.* 1990; Strickland *et al.* 2004b; Veilleux *et al.* 2005). Galactic winds are associated with both star formation (e.g. starbursts), nuclear activity (e.g. FR I radio sources), and a combination of star formation and nuclear activity (e.g. Seyfert galaxies). But this raises many questions. How do winds get going, how energetic are they, how long do they last, and what is their role in galaxy evolution? Do we arrive at similar answers for AGN-driven winds and starburst-driven winds?

Here we are able to shed light on the first question (§5). We have carried out the most detailed and extensive survey to date of extended plasma gas in active galaxies. We constructed ionisation diagnostic diagrams to study the nature of the emission in ten galaxies. We find that the wholly starburst-powered sources have extended emission that is largely consistent with shock ionisation. This sets an important lower limit on the time at which the starburst phenomenon began (≤ 50 Myr). At this time, the stellar UV ionisation sources have long since faded from view which essentially rules out a continuous star formation model for the nucleus, at least in our limited subset of starburst galaxies. An interesting question is whether we can identify those sources that are in an early starburst phase and before the onset of the large-scale wind.

The second question presents difficulties for us, at least in the present analysis. In all of our AGN sources, there is evidence of circumnuclear star formation: the present data are unable to establish which source of activity is responsible for the wind. In future studies, it may be possible to shed light on this question in one of two ways. X-ray spectroscopy can, in principle, establish the $[\alpha/\text{Fe}]$ abundance ratio of the outflowing gas. Enhanced α abundances implicate the presence of SN II, and therefore the central importance of the starburst in driving the outflow. Such an effect may have already been seen in dwarf starburst galaxies (Martin *et al.* (2002), Ott, Walter & Brinks (2005)), but we are unaware of similar studies in Seyfert outflow sources. This is an important avenue for future research.

An alternative approach is to carefully trace the pressure changes over the circumnuclear regions down to small galactic radii. O'Connell & Mangano (1978) noticed that the gas densities, as measured from the [SII] doublet, appear to decrease along the minor axis of M82. Chevalier & Clegg (1985) interpreted this observation as a change of wind pressure in a starburst-driven wind. This idea has been explored extensively by Heckman *et al.* (1990) who used the [S II] doublet to measure the electron densities as a function of radius in a subset of starburst galaxies. In M82, high pressures have been inferred from the [S III] doublet (Houck *et al.* (1984), Smith *et al.* (2006)), from fine structure lines in the far infrared (Lugten *et al.* 1986; Duffy *et al.* 1987), and from the non-thermal radio continuum (Schaaf *et al.* 1989). After certain assumptions, pressures can be inferred by combining observations of radio recombination lines and the associated free-free emission (Rodriguez & Chaisson 1980; Seaquist, Bell & Bignell 1985). The intrinsically higher resolution of linked radio receivers should allow the pressure profile to be traced to the smallest VLBI spatial scales. Naively, the pressure profile can be relatively steep closer to the black hole compared to an anticipated flatter profile across the energy injection region of a starburst (Chevalier & Clegg 1985). Thus, we may be able to distinguish between AGN-powered vs. starburst-powered momentum by measuring the gas pressure as a function of galactocentric radius. We leave this to future work.

In the case of the AGN sources, we find that the extended line emission is always powered by the accretion disk rather than by shock ionisation. Some of these sources are clearly associated with central starbursts that may well contribute momentum to the outflow in which case age-dating the onset of the outflow is more problematic. In the case of the AGN-driven outflow, these could have commenced as recently as 10 Myr or so, although if the starburst dominates, the longer timescale is preferred. The latter case is interesting because it would indicate that the AGN source has a lifetime approaching 100 Myr, and that the amount of gas converted to energy is of order $10^8 \ M_\odot$.

In the next paper, we combine the ionisation diagnostics with the emission-line kinematics to learn more about the energetics of the outflowing gas. The integral field spectrograph approach is clearly very powerful for studying extended emission line sources. We stress that our methods for deriving and comparing ionisation and dynamic timescales can be extended to a wider class of active galaxies (e.g. quasar hosts), mergers (e.g. ULIRGs) and star-forming galaxies (e.g. dwarf irregulars). It will be interesting to compare the inferred timescales with the star formation histories extracted from circumnuclear stellar populations. In high-redshift galaxies where stellar populations are harder to observe, the ionisation diagnostics may provide key information. In the Appendix, we include a brief discussion about how future studies can be improved to advance this work further.

Aeronautics and Space Administration.

Facilities: AAT (AAOmega-SPIRAL)

REFERENCES

Annibali, F., Greggio, L., Tosi, M., Aloisi, A., Leitherer, C. 2003, AJ, 126, 2752
Avedisova, V.S., 1972, SvA, 15, 708
Baldwin J.A, Phillips M.M, & Terlevich R.1981 PASP 93 5
Baldwin J.A, Phillips M.M, & Terlevich R.1981 PASP 93 817
Begelman, M.C. & Bland-Hawthorn, J., 1997, Nature, 385, 22
Bergeron, J., Durret, F., Boksenberg, A, 1983, A&A, 127, 322
Blanco, V.M., Graham, J.A., Lasker, B.M., Osmer, P.S., 1975 ApJ, 198, L63
Bland, J., Taylor, K., Atherton, P.D., 1987 MNRAS, 228, 595
Bland, J. & Tully, B., 1988, Nature, 334, 43
Bland-Hawthorn, J., Wilson, A.S., Tully, R.B., 1991, ApJ, 371L, 19
Bland-Hawthorn, J., & Cohen, M. 2003, ApJ, 582, 246
Bland-Hawthorn, J., & Kedziora-Chudczer, L., 2003, PASA, 20, 242
Bland-Hawthorn, J., & Maloney, P.R., 1999, ApJ, 510L, 33
Bland-Hawthorn, J., Veilleux, S., Cecil, G.N., Putman, M.E., Gibson, B.K., Maloney, P.R., 1998 MNRAS, 299, 611
Burbidge, E.M., Burbidge, G.R., 1960, ApJ, 132, 30
Buzzoni, A., 2005, MNRAS, 361,725,
Carretta, E., Bragaglia, A., & Gratton, R. 2007, A&A, 473, 129
Castor, J., McCray, R., Weaver, R., 1975, ApJ, 200L, 107
Cavaliere, A., & Padovani, P., 1988, ApJ, 333L 33
Cecil, G., Bland, J., Tully, R.B., 1990, ApJ, 355, 70
Cecil, G., Bland-Hawthorn, J., Veilleux, S., 2002, ApJ, 576, 745
Cecil, G., Bland-Hawthorn, J., Veilleux, S., Filippenko, A.V., 2001 ApJ, 555, 338
Cen, R., & Ostriker, J. P. 1999, ApJ, 514, 1
Chevalier, R.A., Clegg, A.W. 1985 Natur 317 44
Coccato, L., Corsini, E.M., Pizzella, A., Morelli, L., Funes, J.G., Bertola, F., 2004, A&A, 416, 507
Colbert, E.J.M., Wilson, A.S., & Bland-Hawthorn, J., 1994, ApJ, 436, 89
Colina, L.; Sparks, W. B.; Macchetto, F. 1991ApJ...370..102C
Collins, J. A., Shull, J. M., & Giroux, M. L. 2007, ApJ, 657, 271
Condon, J.J., Condon, M.A., Gisler, G., Puschell, J.J., 1982 ApJ, 252 102
Cooper, J.L., Bicknell, G.V., Sutherland, R.S., Bland-Hawthorn, J., 2008, ApJ, 674, 157
Dalcanton, J. J. 2007, ApJ, 658, 941
Davé, R., Oppenheimer, B. D., & Sivanandam, S. 2008, MNRAS, 391 110
Demoulin, M.H., Burbidge, E.M., 1970, ApJ, 159, 799
de Zeeuw, P.T., Bureau, M., Emsellem, E., Bacon, R., Carollo, C.M., Copin, Y., Davies, R.L., Kuntschner, H., *et al.*, 2002, MNRAS, 329 513
Dopita, M.A., Sutherland, R.S., 1996, ApJS, 102 161
Duffy, P.B., Erickson, E.F., Haas, M.R., Houck, J.R., 1987, ApJ, 315, 68
Edmunds, M.G., & Pagel, B.E.J., 1982 MNRAS 198 1089
Efstathiou, G. 2000, MNRAS, 317, 697
Erb, D. K. *et al.*2006, ApJ, 647, 128
Fall, S. M. 2002, in Disks of Galaxies: Kinematics, Dynamics and Perturbations, ASP Conf. Series, Vol. 275, ed. E. Athanassoula, A. Bosma, & R. Mujica (San Francisco: ASP), p. 389
Fabbiano, G., Heckman, T., Keel, W.C., 1990, ApJ, 355, 442
Flohic, H.M.L.G., Eracleous, M., Chartas, G., Shields, J.C., Moran, E.C., 2006, ApJ, 647, 140
Forbes, D.A., Boisson, C., & Ward, M.J., 1992, MNRAS, 259, 293
Forbes, D.A., & Norris, R.P. 1998, MNRAS, 300, 757
Freeman, K.C., Karlsson B., Lynga, G., Burrell, J.F., van Woerden, H., Goss, W.M., Mebold, U., 1977, A&A, 55, 445
Fox, A. J., Wakker, B. P., Savage, B. D., Tripp, T. M., Sembach, K. R., & Bland- Hawthorn, J. 2005, ApJ, 630, 332
Genzel, R., Burkert, A., Bouché, N., Cresci, G., Förster Schreiber, N.M., Shapley, A., Shapiro, K., Tacconi, L.J. *et al.*, 2008, ApJ, 687, 59
Greenhill, L.J., Booth, R.S., Ellingsen, S.P., Herrnstein, J.R., Jauncey, D.L., McCulloch, P.M., Moran, J.M., Norris, R.P., Reynolds, J.E., Tzioumis, A.K. 2003, ApJ, 590, 162
Greenhill, L.J., Kondratko, P.T., Lovell, J.E.J., Kuiper, T.B.H., Moran, J.M., Jauncey,D.L., Baines, G.P., 2003 ApJ, 582L, 11
Greve, A., 2004, A&A, 416, 67
Grimes, J.P., Heckman, T., Aloisi, A., Calzetti, D., Leitherer, C., Martin, C.L., Meurer, G., Sembach, K., Strickland, D. 2009, ApJS, 181, 272
Hameed, S., Devereux, N., 1999, AJ, 118, 730
Heckman, T.M, Armus, L.M., Miley, G.K., 1990, ApJS, 74, 833

Heckman, T.M., Robert., Leitherer, C., Garnett, D.R., van der Rydt, F., 1998, ApJ, 503, 646
Hjelm, M., Lindblad, P.O., 1996, A&A, 305, 727
Holtzman, J. A. et al., 1993, AJ, 106, 1826
Hoopes, C.G., Heckman, T.M., Strickland D.K., Seibert, M. Madore, B.F., Rich, R.M., Bianchi, L., Gil de Paz, A., 2005 ApJ, 619L 99
Houck, J.R., Shure, M.A., Gull, G.E., Herter, T., 1984, ApJ, 287L, 11
Hunter, D.A., Hawley, W.N., & Gallagher, J.S. iii, 1993, AJ, 106, 1797
Irwin, J.A., Sofue, Y., 1996, ApJ, 464, 738
Israel, F.P., 1998, A&ARv, 8 237
Jiménez-Bailón, E., Santos-Lleó, M., Dahlem, M., Ehle, M., Mas-Hesse, J.M., Guainazzi, M., Heckman, T.M., Weaver, K.A. 2005, A&A, 442, 861
Junkes, N., Zinnecker, H., Hensler, G., Dahlem, M., Pietsch, W., 1995, A&A, 294, 8
Jöersäeter, S. Peterson, C.J., Lindblad, P.O., Boksenberg, A., 1984, A&AS, 58, 507
Keeney, B. A., Danforth, C. W., Stocke, J. T., Penton, S. V., Shull, J. M., & Sembach, K. R. 2006, ApJ, 646, 951
Kewley L.J., Dopita M.A., Sutherland R.S., Heisler C.A. & Trevena J. 2001 ApJ 556 121
Kirby, E. N., Simon, J. D., Geha, M., Guhathakurta, P., & Frebel, A. 2008, ApJ, 685, L43
Krabbe, A., Sternberg, A., Genzel, R., 1994, ApJ, 425, 72
Krajnović, D., Sharp, R. & Thatte, N., 2007, MNRAS, 374, 385
Komossa, S., Burwitz, V., Hasinger, G., Predehl, P., Kaastra, J.S.,, Ikebe, Y. 2003 ApJ 582L 15
Koo, B.-C., & McKee, C.F., 1992a, ApJ, 388, 93
Koo, B.-C., & McKee, C.F., 1992b, ApJ, 388, 103
Kraft, R.P., Hardcastle, M.J., Sivakoff, G.R., Jordán, A., Nulsen, P.E.J., Birkinshaw, M., Forman, W.R., Jones, C., *et al.* 2008 ApJ, 677L 97
Lada, C.J., & Lada, E.A., 2003, ARA&A, 41, 57
Leitherer, C., Robert, C., Drissen, L., 1992, ApJ, 401, 596 A&A, 467, 283
Lehnert, M.D., & Heckman, T.M. 1996, ApJ, 462, 651
Lugten, J.B., Watson, D.M., Crawford, M.K., Genzel, R., 1986, ApJ, 311L, 51
Laurent, O., Mirabel, I.F., Charmandaris, V., Gallais, P., Madden, S.C., Sauvage, M., Vigroux, L., Cesarsky, C., 2000, A&A, 359, 887
Lutz, D., Maiolino, R., Moorwood, A.F.M., Netzer, H., Wagner, S.J., Sturm, E., Genzel, R., 2002, A&A, 396, 439
Mac Low, M.-M.& McCray, R., 1988, ApJ, 324, 776
Madau, P., Ferrara, A., & Rees, M. J. 2001, ApJ, 555, 92
Maloney, P.R., 1999, Ap&SS, 266, 207
Martin, C.L., 2006, ApJ, 647, 222
Martin, C. L., Kobulnicky, H. A., & Heckman, T. M. 2002, ApJ, 574, 663
Matt, G., Fabian, A.C., Guainazzi, M., Iwasawa, K., Bassani, L., Malaguti, G., 2000, MNRAS318, 173
McCarthy, P.J., van Breugel. W., Heckman, T., 1987 AJ, 93, 264
Meurer, G.R., Freeman, K.C., Dopita, M.A.. Cacciari C., 1992, AJ, 103, 60
Morganti, R., Holt, J.,Saripalli, L., Oosterloo, T.,A., & Tadhunter C.N. 2007 A&A 476 723
Morganti, R., Oosterloo, T., Tsvetanov, Z, 1998, AJ, 115, 915
Mueller-Sánchez, F., Davies, R.I., Eisenhauer, F., Tacconi L.J., Genzel, R., Sternberg, A., 2006, A&A, 454, 481
Norman, C., Silk, J., 1983, ApJ, 266, 502
Navarro, J. F., & White, S. D. M. 1994, MNRAS, 267, 401
Nicholson, R.A., Bland-Hawthorn, J.; Taylor, K., 1992 ApJ, 387, 503
O'Connell, R.W., & Mangano, J.J., 1978, ApJ, 221, 62
Oliva, E., Salvati, M., Moorwood, A.F.M., Marconi A., 1994, A&A, 288, 457
Osterbrock, D.E., "Astrophysics of Gaseous Nebulae and Active Galactic Nuclei", University Science Books
Ott, J., Walter, F., & Brinks, E., 2005, MNRAS, 358, 1453
Persic, M., Mariani, S., Cappi, M., Bassani, L., Danese, L., Dean, A.J., di Cocco, G., Franceschini, A., *et al.*, 1998, A&A, 339L 33
Peterson, B.A., Dickens, R.J., Cannon, R.D.m 1975, PASAu, 2, 366
Phillips, A.C., 1993, AJ, 105, 486
Phillips, M.M., Edmunds, M.G., Pagel, B.E.J., Turtle, A.J., 1983, MNRAS, 203, 759
Pogge, R.W. & Eskridge, P.B., 1987, AJ, 93, 291

Ptak, A., Heckman, T., Levenson, N.A., Weaver, K., Strickland, D., 2003, ApJ, 592, 782

Quillen, A.C., Brookes, M.H., Keene, J., Stern, D., Lawrence, C.R., Werner, M.W., 2006,ApJ, 645, 1092

Quillen, A.C., Graham, J.R., Frogel, J.A., 1993, ApJ, 412, 550

Rand, R.J., 1998, ApJ, 501, 137

Rice, W., Lonsdale, C.J., Soifer, B.T., Neugebauer, G., Kopan, E.L., Lloyd, L.A., de Jong, T., Habing, H.J., 1988 ApJS, 68, 91

Rieke, G.H., Lebofsky, M.J., Thompson, R.I., Low, F.J., Tokunaga, A.T., 1980, ApJ, 238, 24

Robertson, B. et al. 2006, ApJ, 645, 986

Rodriguez, L.F. & Chaisson, E.J., 1980, ApJ, 238, 41

Ryan-Weber, E. V., Pettini, M., & Madau, P. 2006, MNRAS, 371, L78

Saunders, W., Bridges T., Gillingham, P., *et al.*, 2004, SPIE, 5492, 389

Sakamoto, K., Ho, Paul T.P., Iono, D., Keto, E.R., Mao, R., Matsushita, S., Peck, A.B., Wiedner, M.C., Wilner, D.J., Zhao, J. 2006 ApJ, 636, 685

Sandqvist, Å., Jöersäeter, S., Lindblad, P.O., 1995, A&A, 295, 585

Schaaf, R., Pietsch, W., Biermann, P.L., Kronberg, P.P., Schmutzler, T., 1989, ApJ, 336, 722

Schmelz, J. T.; Baan, W. A.; Haschick, A. D. 1987, ApJ, 320 145

Schmelz, J. T.; Baan, W. A.; Haschick, A. D. 1987, ApJ, 315 492

Schiano, A.V.R., 1985, ApJ, 299, 24

Schwartz, C.M., & Martin, C.L., 2004, ApJ, 610, 201

Schwartz, C.M., Martin, C.L., Chandar, R., Leitherer, C., Heckman, T.M., Oey, M.S. 2006, ApJ, 646, 858

Seaquist, E.R., Bell, M.B., Bignell, R.C., 1985, ApJ, 294, 546

Sedov, L.I., 1958, RvMP, 30, 1077

Sharp, R.G., *et al.*, 2006, SPIE, 6269E, 14

Shopbell, P.L. & Bland-Hawthorn, J., 1998, ApJ, 493, 129

Shull & McKee, 1979, ApJ, 227, 131

Siebenmorgen, R., Haas, M., Pantin, E., Krü gel, E., Leipski, C., Kä ufl, H.U., Lagage, P.O., Moorwood, A., Smette, A., Sterzik, M. 2008, A&A, 488, 83

Smith, L.J., Westmoquette, M.S., Gallagher, J.S., O'Connell, R.W., Rosario, D.J., de Grijs, R., 2006, MNRAS, 370, 513

Soltan, A., 1982, MNRAS, 200, 115

Steigman, G., Strittmatter, P.A., Williams, R.E., 1975, ApJ, 198, 575

Steinmetz, M., & Müller, E. 1995, MNRAS, 276, 549

Stevens, I.R., Forbes, D.A., Norris, R.P., 1999, MNRAS, 306, 479

Strickland, 2007, MNRAS, 376, 523

Strickland, D.K., Heckman, T.M, Colbert, E.J.M., Hoopes, C.G., & Weaver, K.A., 2004, ApJS, 151, 193

Strickland, D.K., Heckman, T.M., Colbert, E.J.M., Hoopes, C.G., Weaver, K.A., 2004, ApJ, 606, 829

Strickland, D.K., Heckman, T.M., Weaver, K.A., & Dahlem, M. 2000, AJ, 120, 2965

Strickland, D.K., & Heckman, T.M., 2009, ApJ, 697 2030

Strickland, D.K., & Stevens, I.R., 2000, MNRAS, 314, 511

Storchi-Bergmann, T., Bonatto, C.J., 1991 MNRAS, 250, 138

Suchkov, A.A., Balsara, D.S.; Heckman, T.M., Leitherer, C. 1994, ApJ, 430, 511

Sutherland, R.S., Bicknell, G.V., Dopita, M.A., 1993, ApJ, 414, 510

Tadhunter, C. & Tsvetanov, Z., 1989, Nature, 341, 422

Taylor, G., 1950, RSPSA, 201, 159

Terlevich, R., & Melnick, J., 1985, MNRAS 213 841

Tomisaka, K., & Ikeuchi, S., 1988, ApJ, 330, 695

Tremonti, C. A. et al. 2004, ApJ, 613, 898

Tully, B.R., "Nearby galaxies catalog", 1988, Cambridge University Press

Veilleux & Bland-Hawthorn J., 1997, ApJL, 479, 105

Veilleux, S., Cecil, G., Bland-Hawthorn, J. 2005, ARA&A, 43, 769

Veilleux, S., Cecil, G., Bland-Hawthorn, J., Tully, R.B., Filippenko, A.V., Sargent, W.L.W., 1994, ApJ, 433, 48

Veilleux, & Osterbrock, 1987, ApJS, 63, 295

Veilleux S., & Rupke, D.S., 2002, ApJ, 565, 63L

Veilleux, S., Shopbell, P.L., Rupke, D.S., Bland-Hawthorn, J. & Cecil, G., 2003, AJ, 126, 2185

Veron-Cetty, M.-P., & Veron, P, 1985, A&A, 145, 425

Veron, P., Lindblad, P.O., Zuiderwijk, E.J., Veron, M.P., Adam, G., 1980, A&A, 87, 245

Ward, M.J., Wilson, A.S., Penston, M.V., Elvis, M., Maccacaro, T., Tritton, K.P., 1978, ApJ, 223, 788

Weaver , R., McCray, R., Castor, J., Shapiro, P., Moore, R., 1977, ApJ, 218, 377

Westmoquette, M.S., Smith, L.J., Gallagher, J.S., Trancho, G., Bastian, N., Konstantopoulos, I.S., 2009, ApJ, 696, 192

Westmoquette, M.S., Gallagher, J.S., Smith, L.J., Trancho, G., Bastian, N., Konstantopoulos, I.S., 2009, ApJ, 706, 1571

Wilson, Shopbell, Simpson *et al.* 2000, AJ, 120, 1325
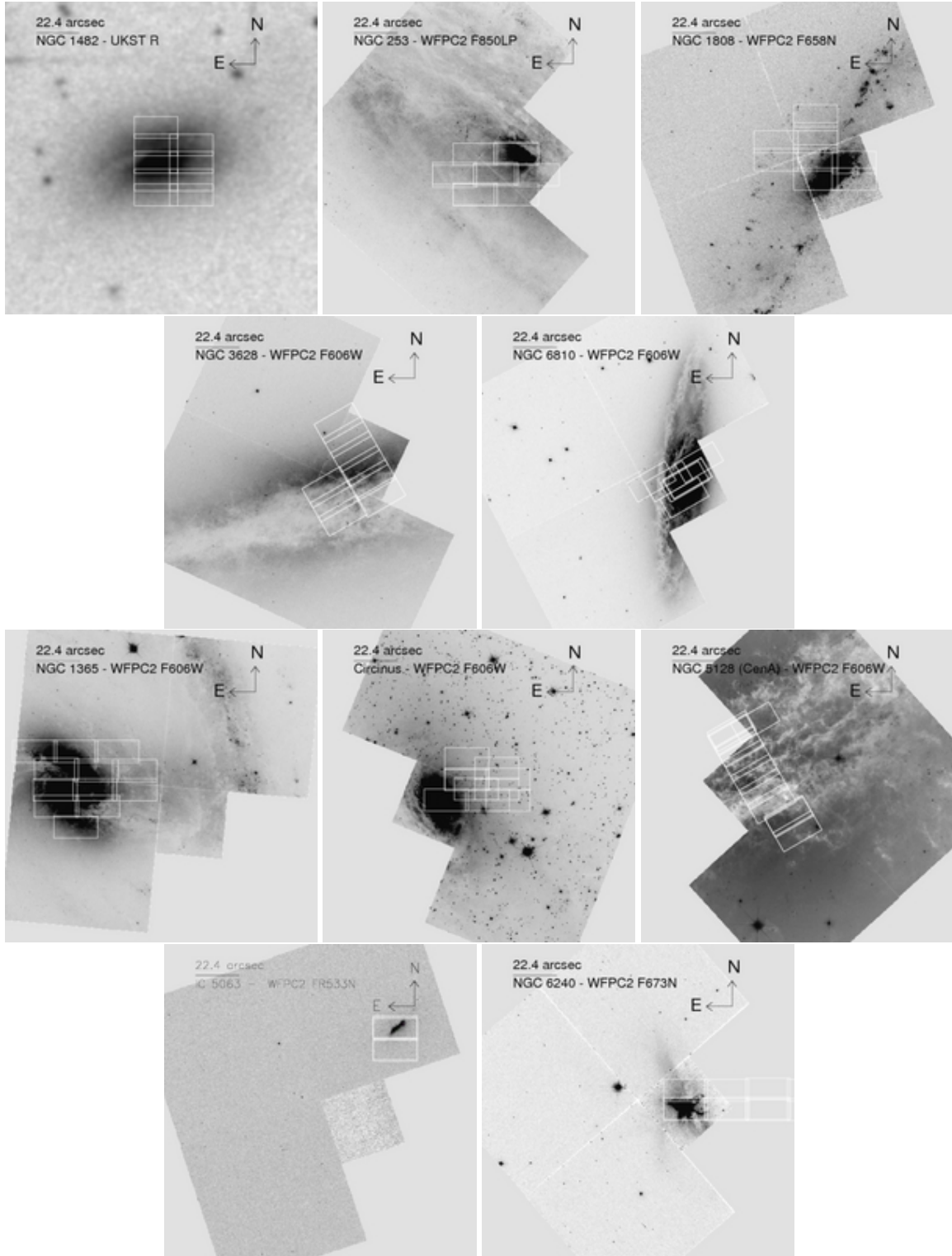
Fig. 1.— SPIRAL IFU footprints. Images are taken from *HST*/WFPC2 associations where available and from the DSS for NGC 1482. The 22.4″ long axis of the SPIRAL IFU is indicated for scale. Note the unusual PA for observations of NGC 6810, NGC 3628 & NGC 5128 due to the detailed requirements of the NGC 5128 observing program during the May 2007 run.
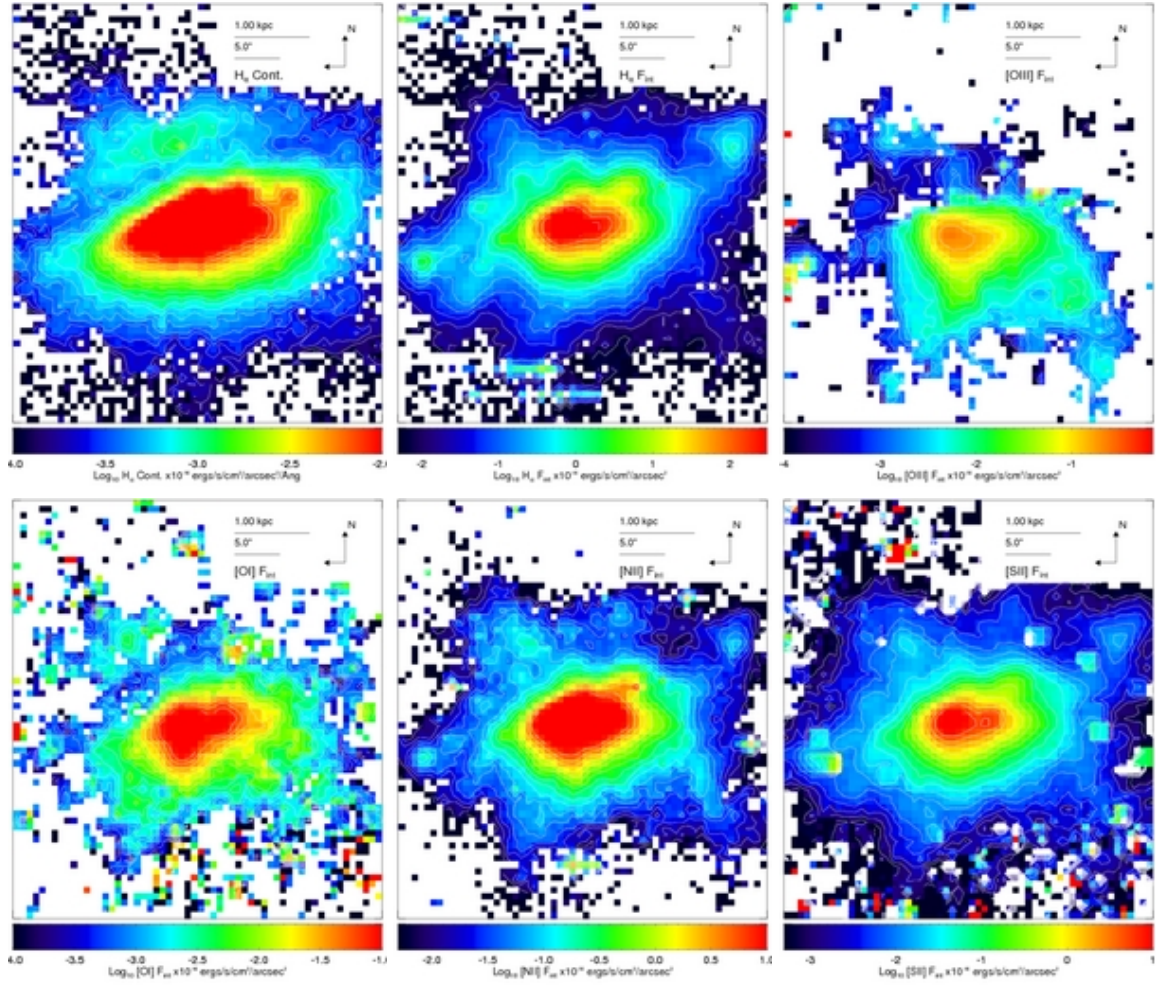
FIG. 2.— NGC 1482: Emission line integrated flux maps are genearted by single gaussian fitting to individual spectra. The maps shown (left to right, top to bottom) are the continuum at line centre for Hα followed by integrated intensity maps (F$_{int}$) for Hα, [O III]λ5007, [O I]λ6300, [N II]λ6583 & [S II]λ6716. Pixels for which no valid fit was obtained are left blank.
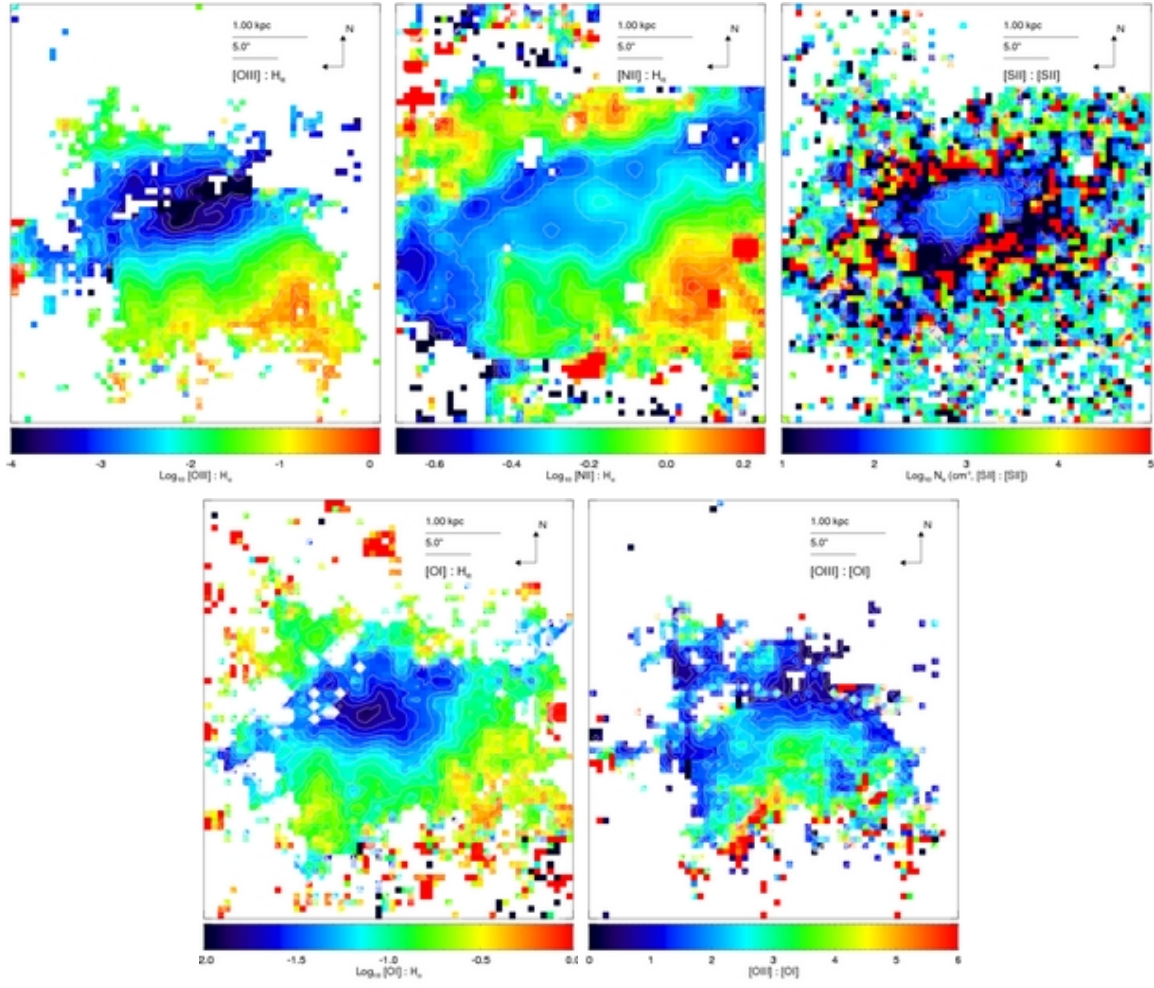
FIG. 3.— NGC 1482: Line ratio maps are constructed from the emission line fits of figure 2. The [S II] ratio is presented as an electron density, N$_e$, following Osterbrock (1988). Pixels without valid measurements in both lines are left blank.
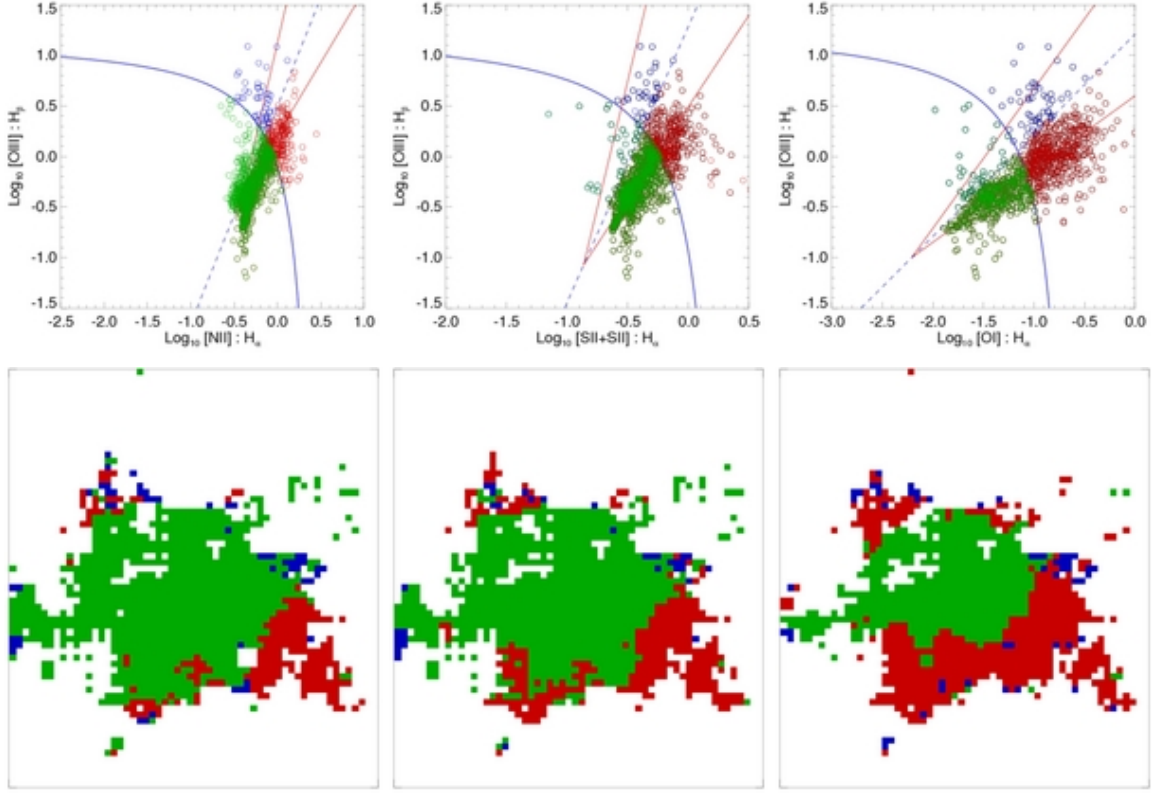
Fig. 4.— NGC 1482: The classic Ionisation Diagnostic Diagrams (IDDs, see section 2.4) are constructed from the integrated line flux measurements. Only IFU mosaic elements with valid line fits for all four (five for [S II]) lines are shown in each case. For each set of line ratios in turn, classification zones are defined and used to reconstruct the spatial distribution of the corresponding gas in the lower figures. The curved solid line marks the *extreme starburst* limit of Kewley *et al.* (2001). Two fiducial indicators are drawn (straight solid lines). The right hand line traces the locus of points for the shock excited emission of NGC 1482 (this galaxy). The left indicator traces the locus of line ratios for the AGN excited emission of NGC 1365 (Fig. 18). The dashed line marks the bisector between these two fiducial traces.
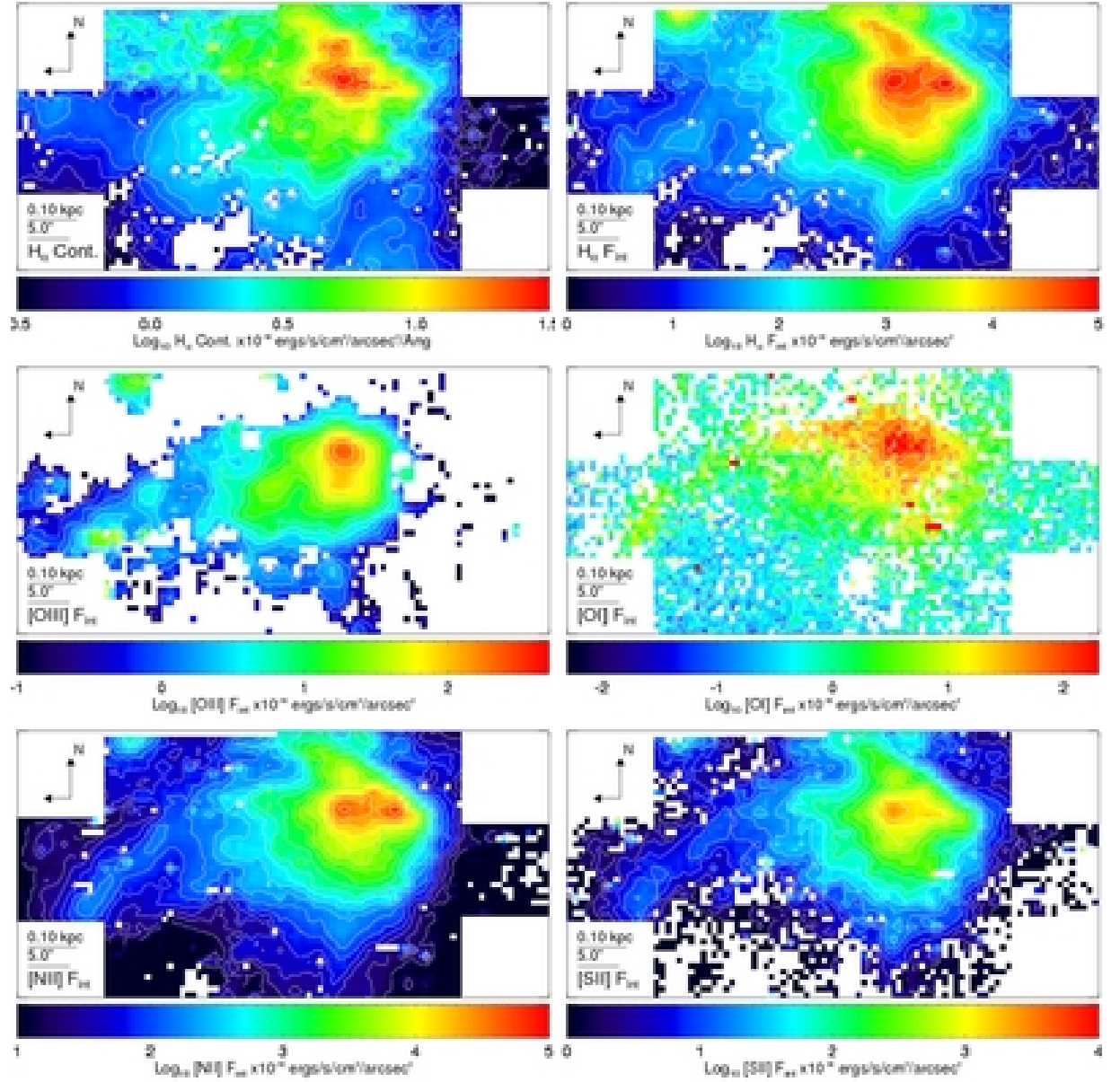
Fig. 5.— NGC 253: Emission line maps are generated as for Fig. 2.
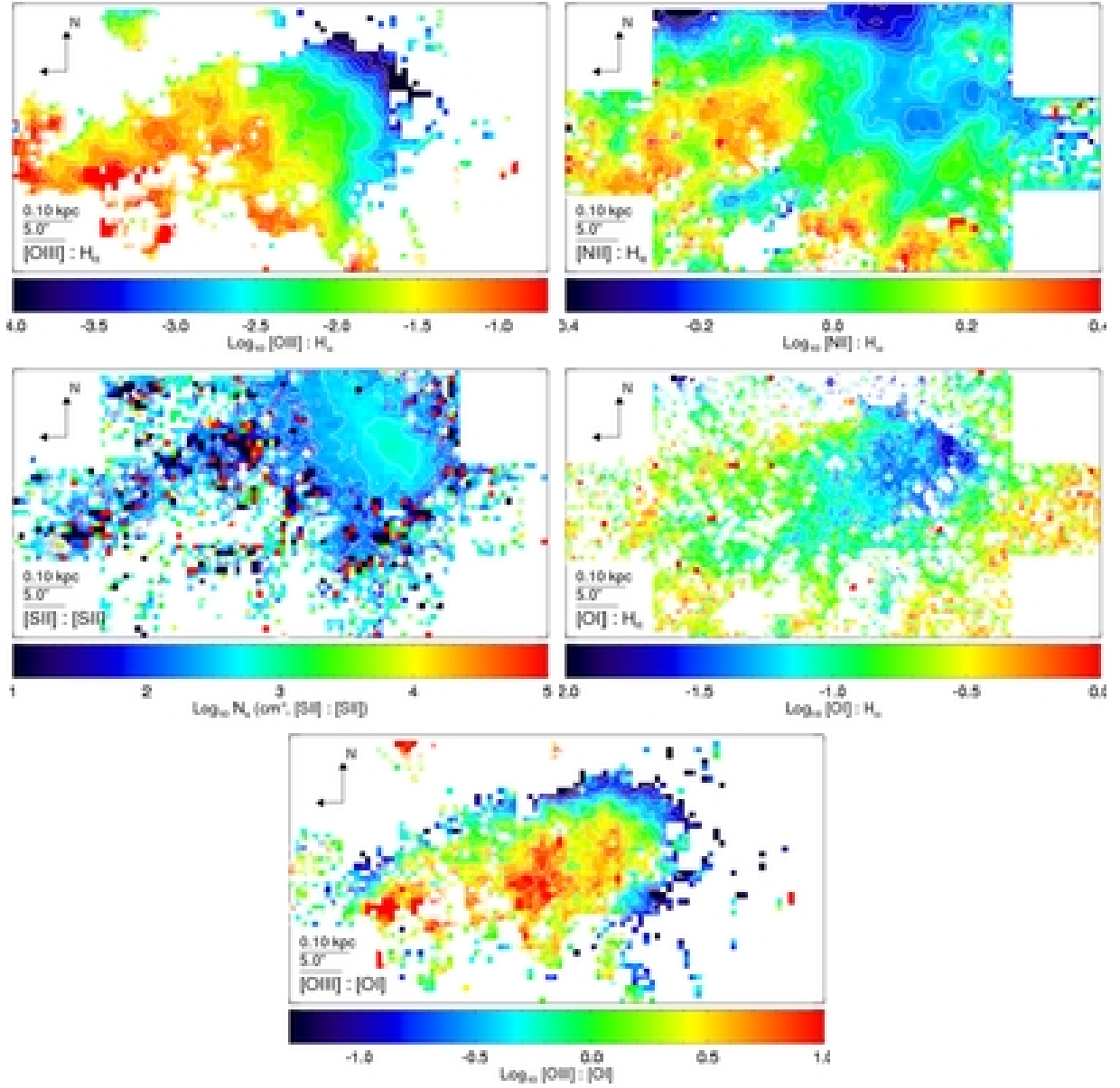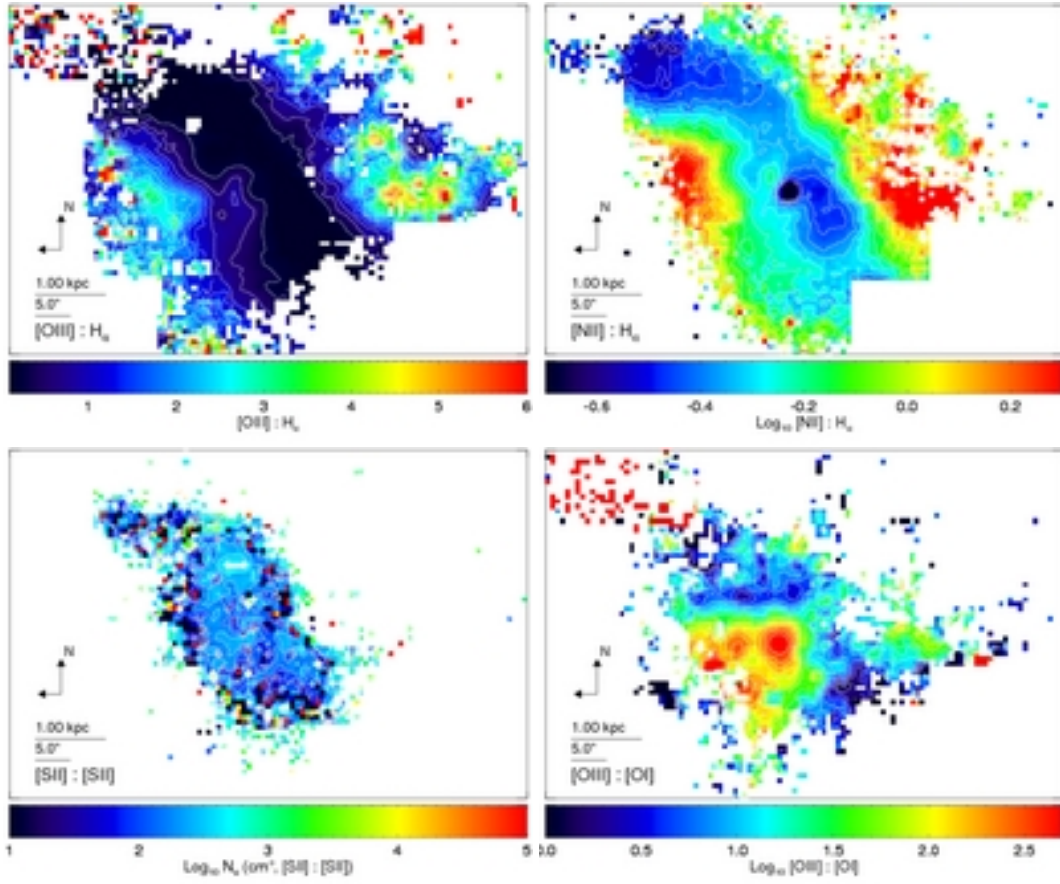
FIG. 6.— NGC 253: Line ratio maps are constructed following Fig. 3.
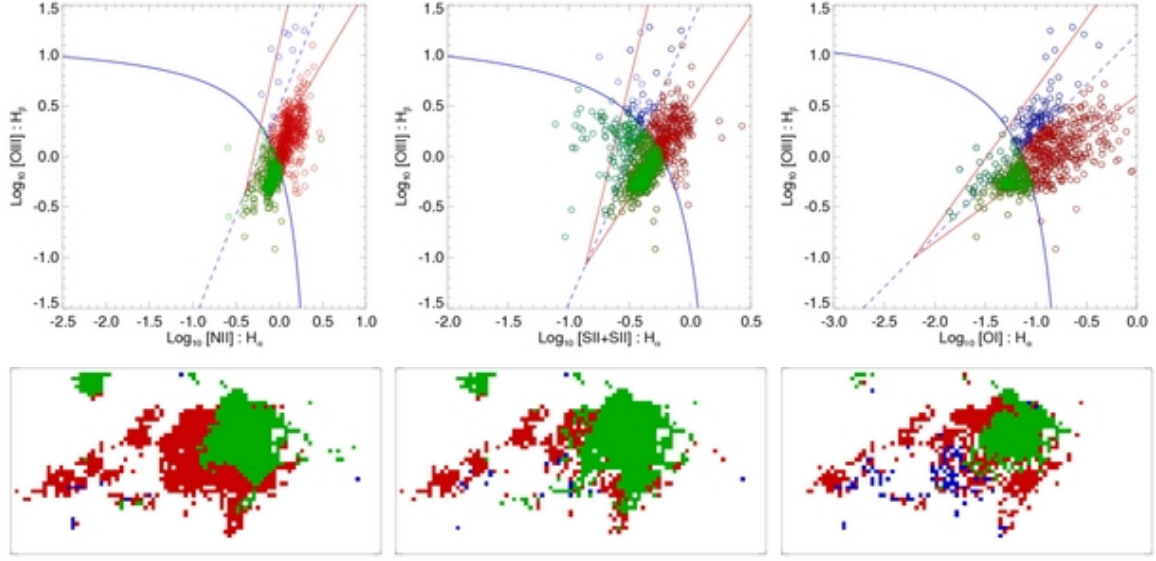
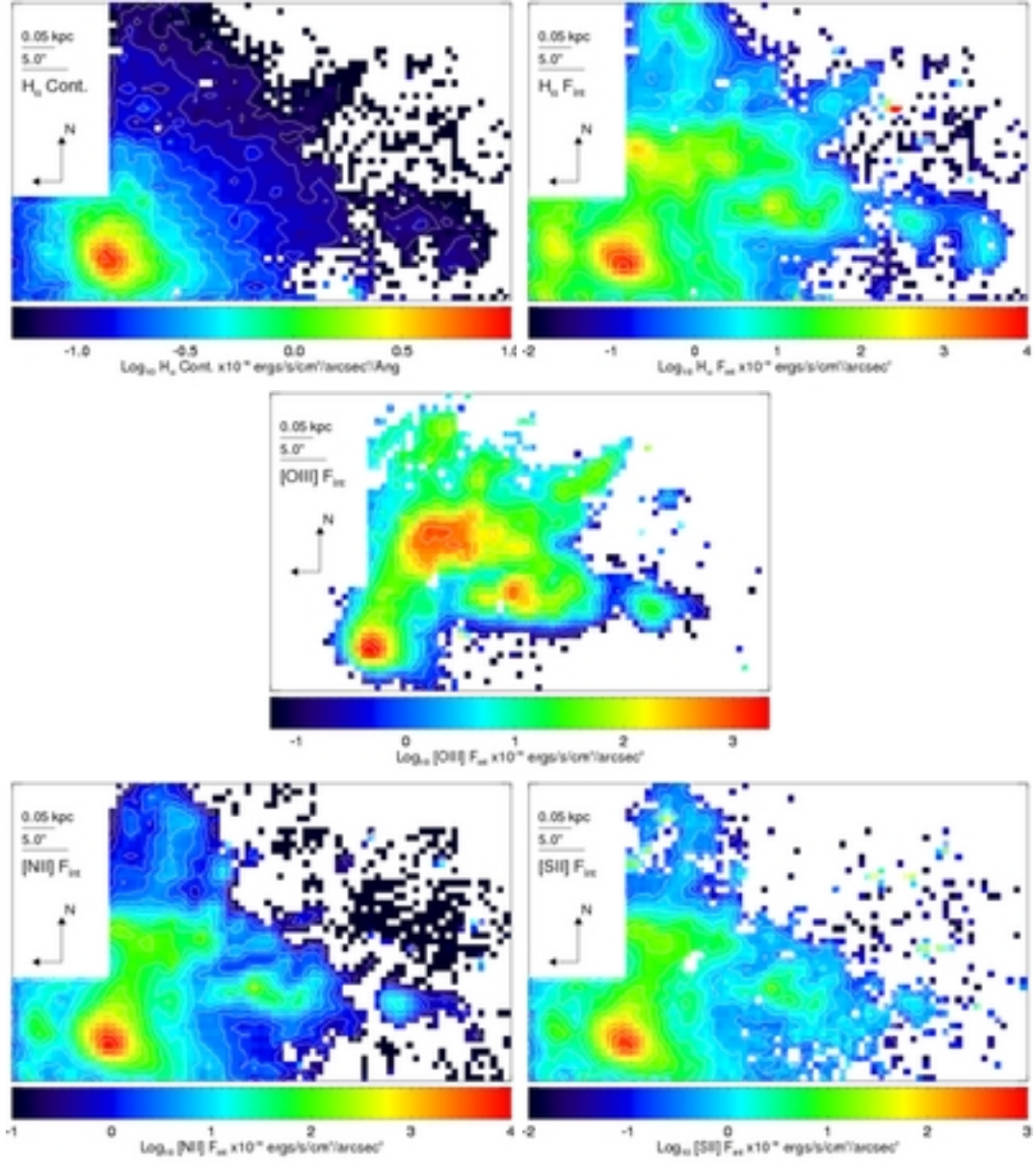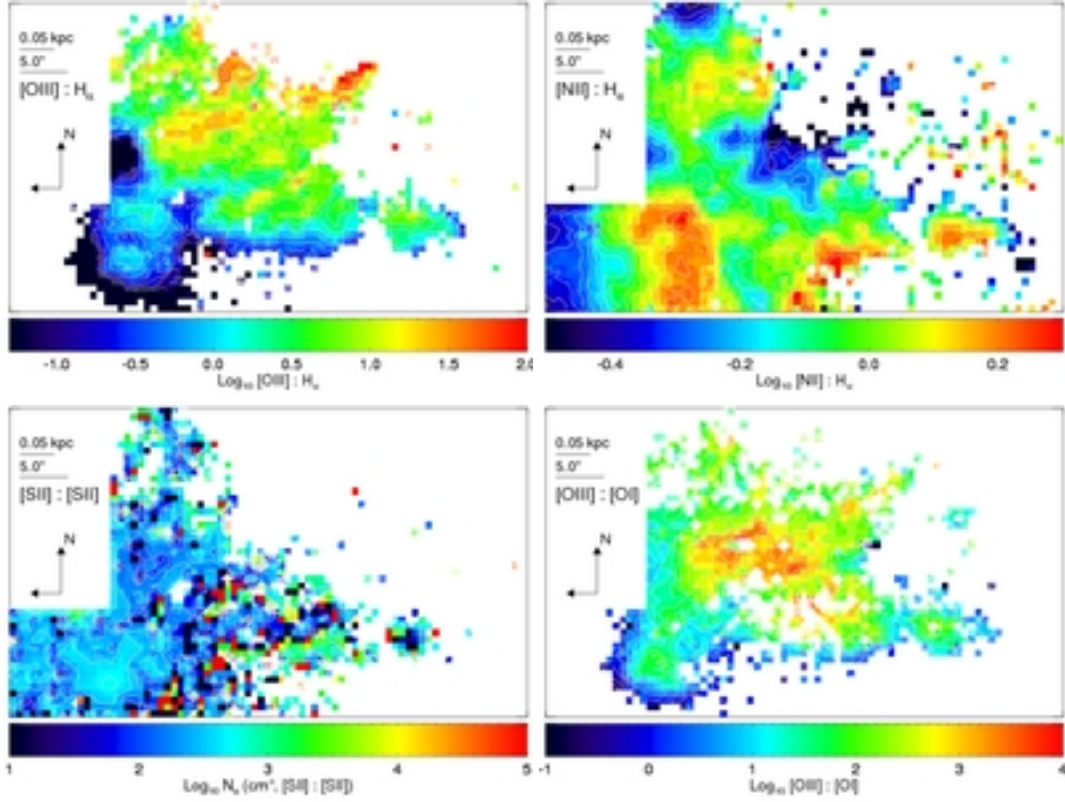FIG. 7.— NGC 253: Ionisation Diagnostic Diagrams are constructed following Fig. 4 and using the same fiducial indicators.
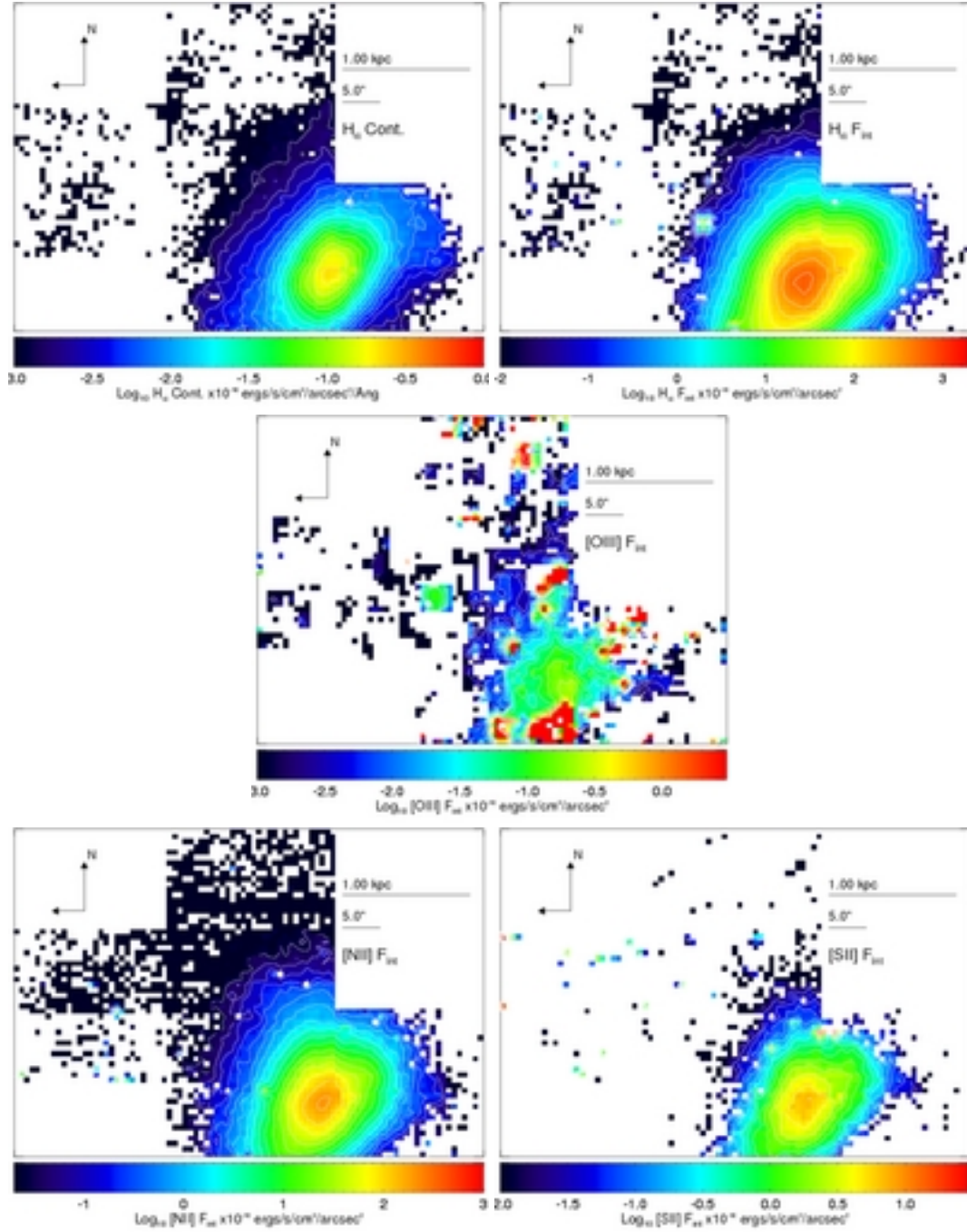
Fig. 8.— NGC 1808: Emission line maps are generated as for Fig. 2. Observations of NGC 1808 were undertaken during a period of poor atmospheric transparency and so emission line maps suffer reduced sensitivity. No [O I] emission was recovered.
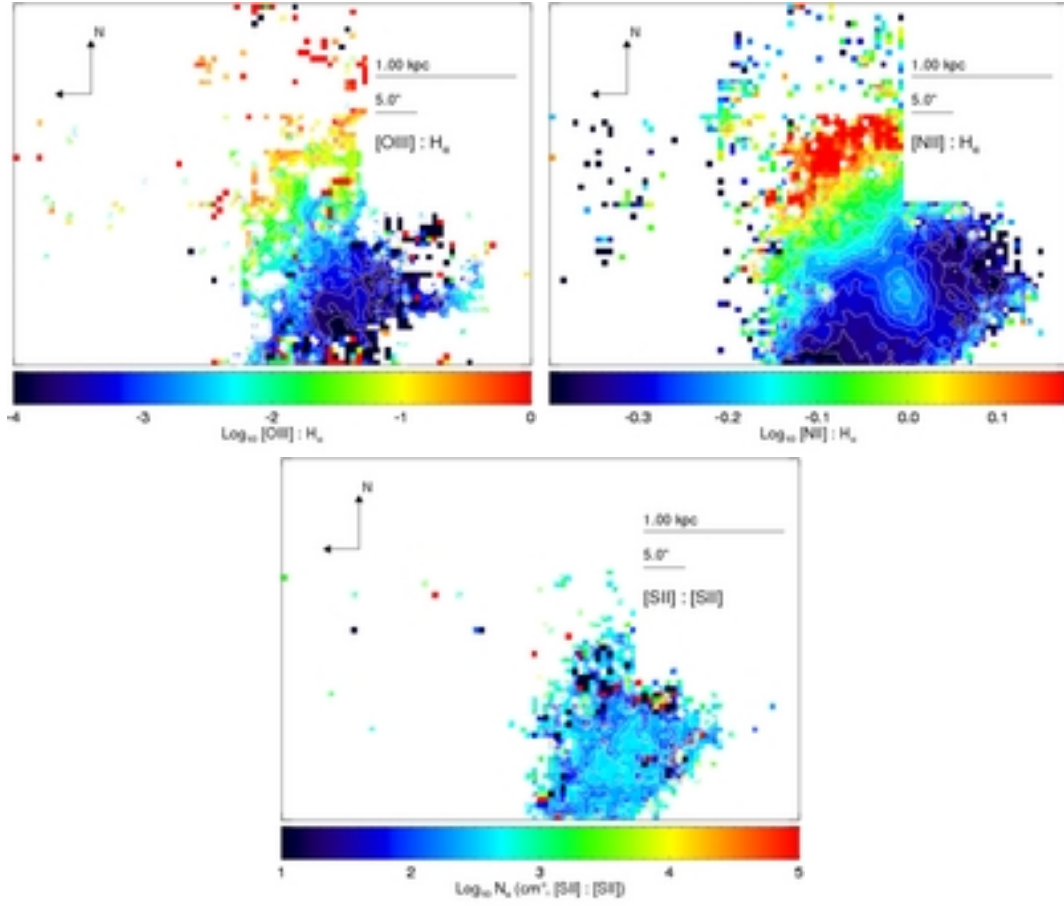
Fig. 9.— NGC 1808: Line ratio maps are constructed following Fig. 3. Observations of NGC 1808 were undertaken during a period of poor atmospheric transparency and so emission line maps suffer reduced sensitivity.
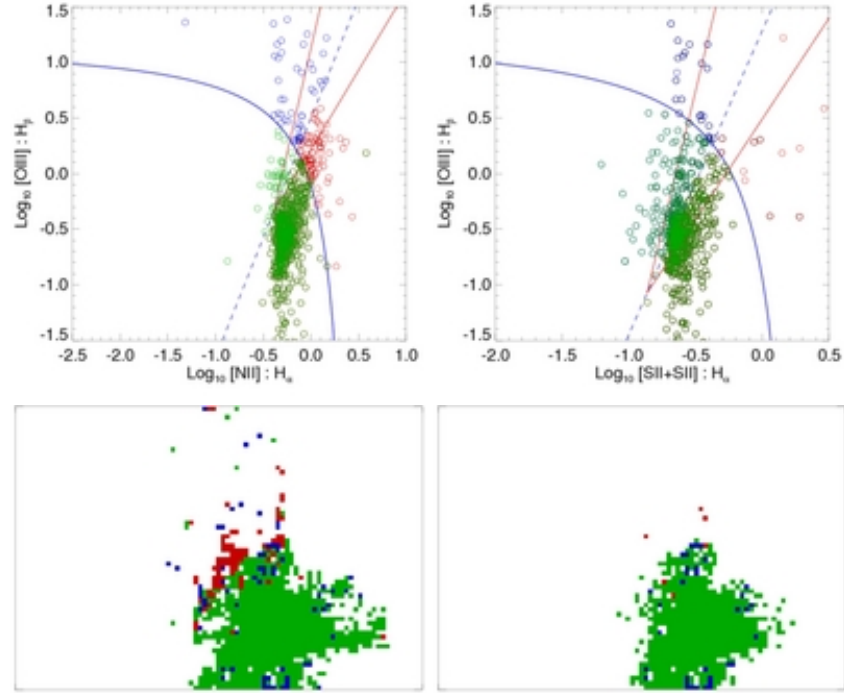
Fig. 10.— NGC 1808: Ionisation Diagnostic Diagrams are constructed following Fig. 4. No [O I] emission was recovred and so the third IDD cannot be constructed.
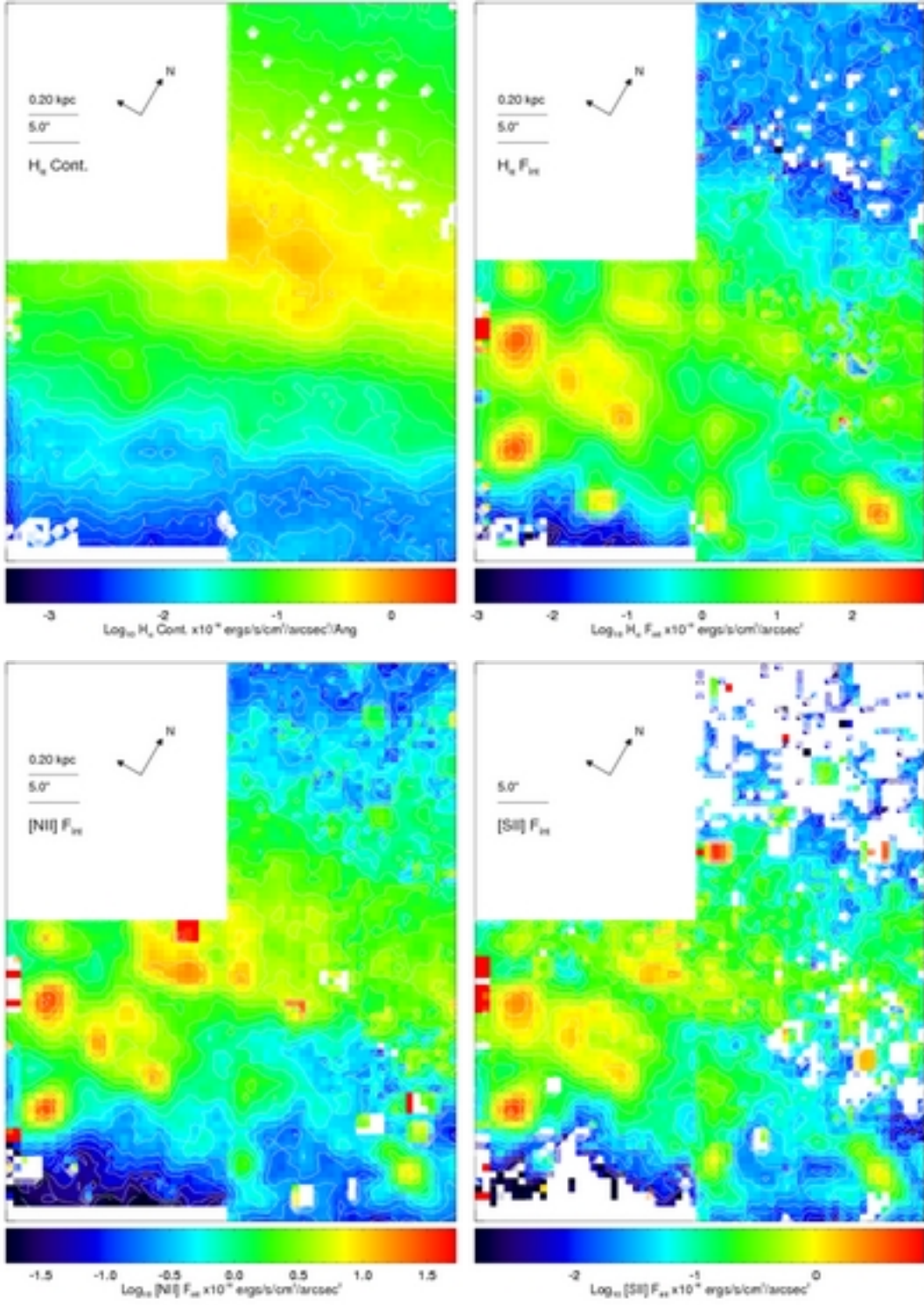
FIG. 11.— NGC 3628: Emission line intensity maps following Fig. 2. Observations of NGC 3628 were undertaken during a period of poor atmospheric transparency and so emission line maps suffer reduced sensitivity. No [O I] emission was recovered.
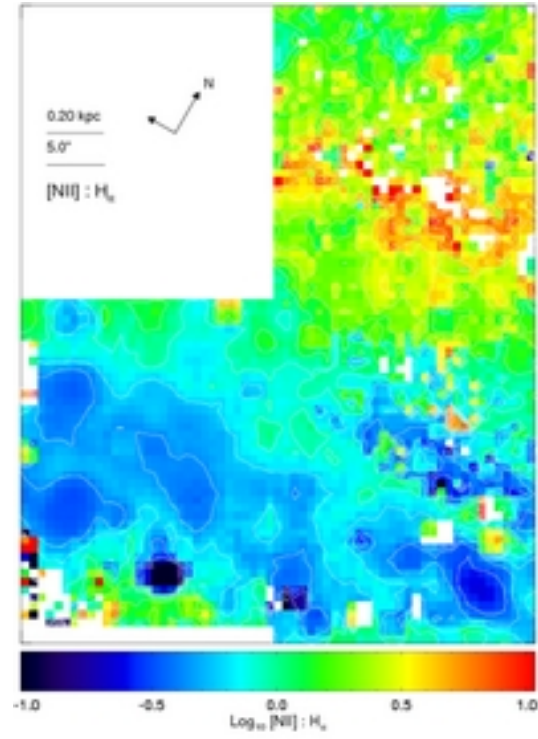
FIG. 12.— NGC 3628: Line ratio maps are constructed following Fig. 3. Due to the reduce sensitivity of the observations for NGC 3628, only the [N II]/Hα map is recovered.
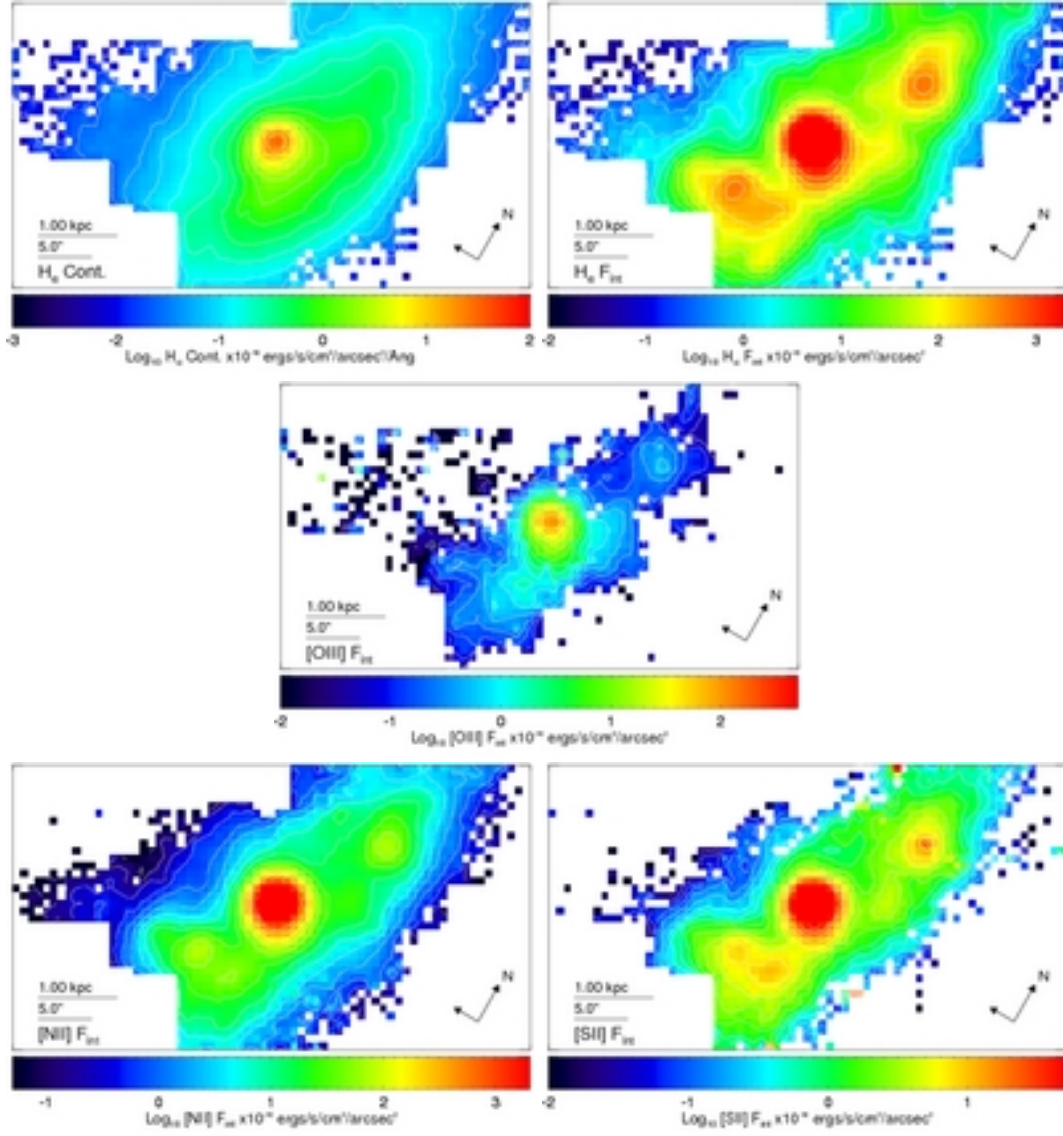
FIG. 13.— NGC 6810: Emission line intensity maps following Fig. 2. The [O III] map is limited in extent by the sensitivity of the data, and no [O I] map was recovered.
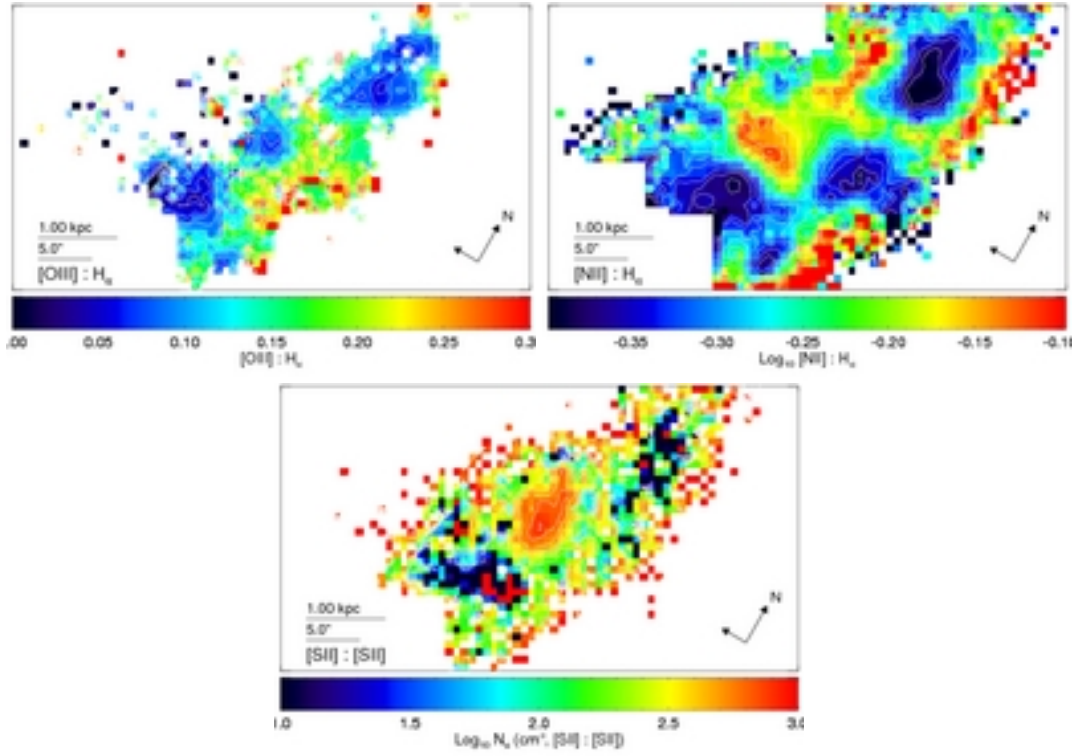
FIG. 14.— NGC 6810: Line ratio maps are constructed following Fig. 3.
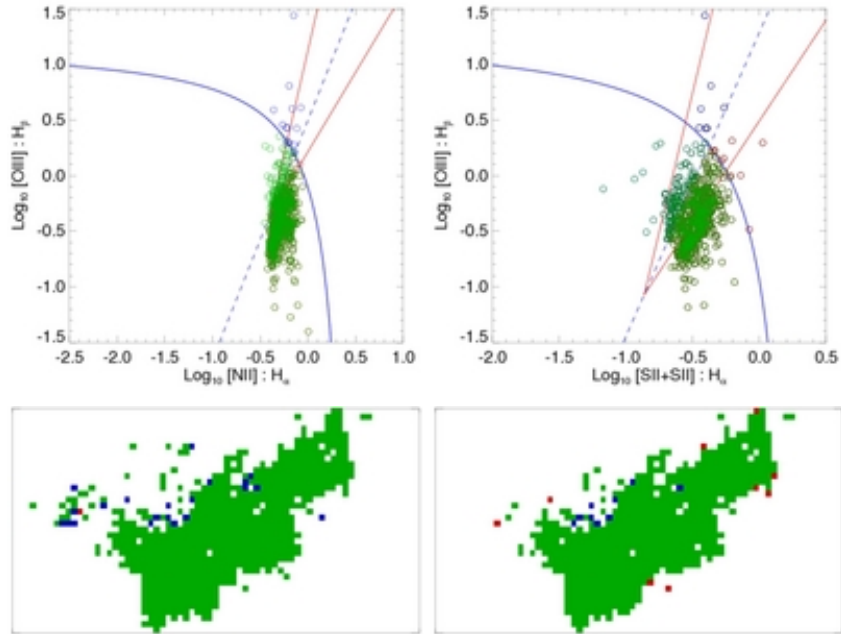
FIG. 15.— NGC 6810: Ionisation Diagnostic Diagrams are constructed following Fig. 4. No [O I] emission was recovred and so the third IDD cannot be constructed for NGC 6810.
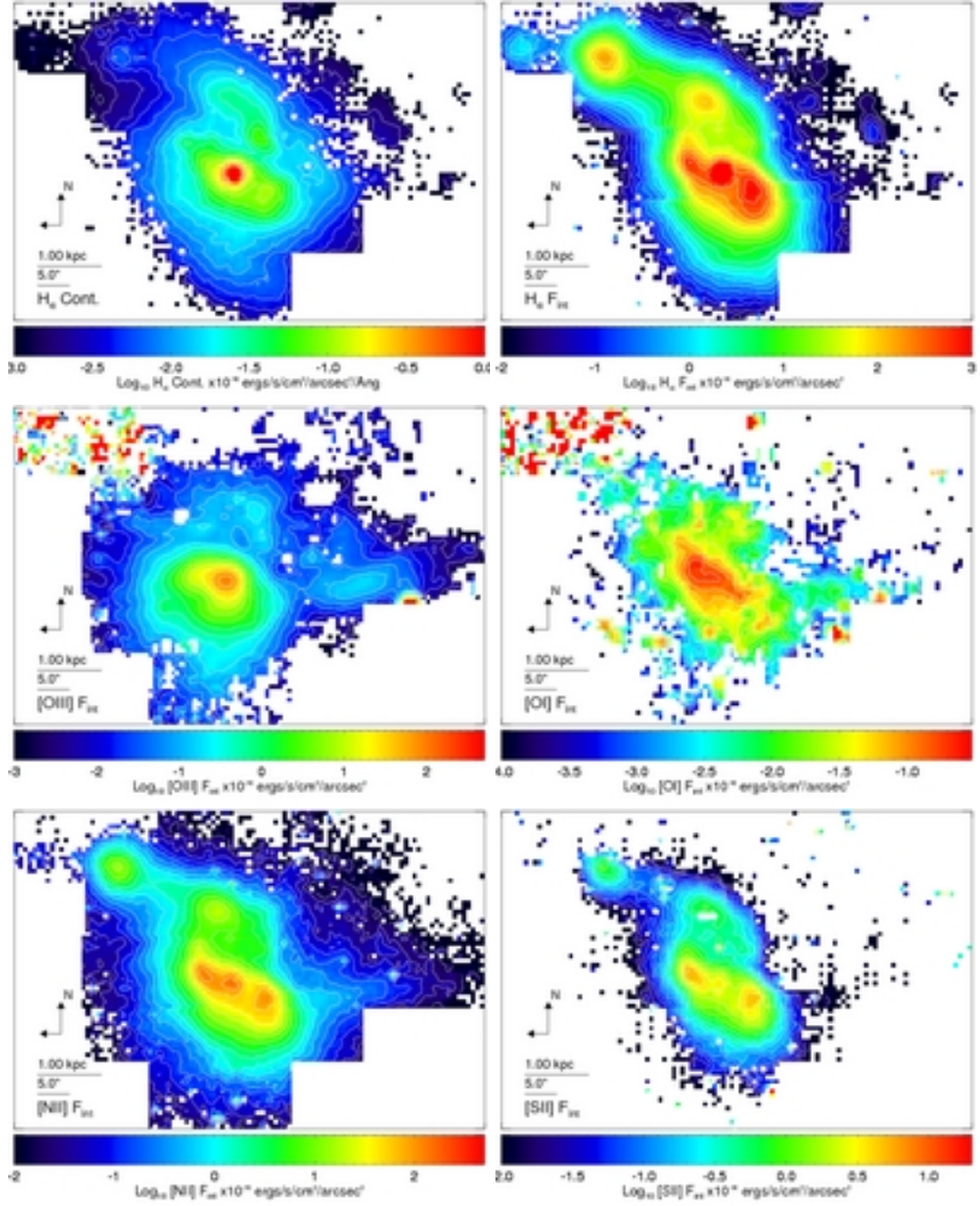
Fig. 16.— NGC 1365: Emission line intensity maps following Fig. 2.

FIG. 17.— NGC 1365: Line ratio maps are constructed following Fig. 3.
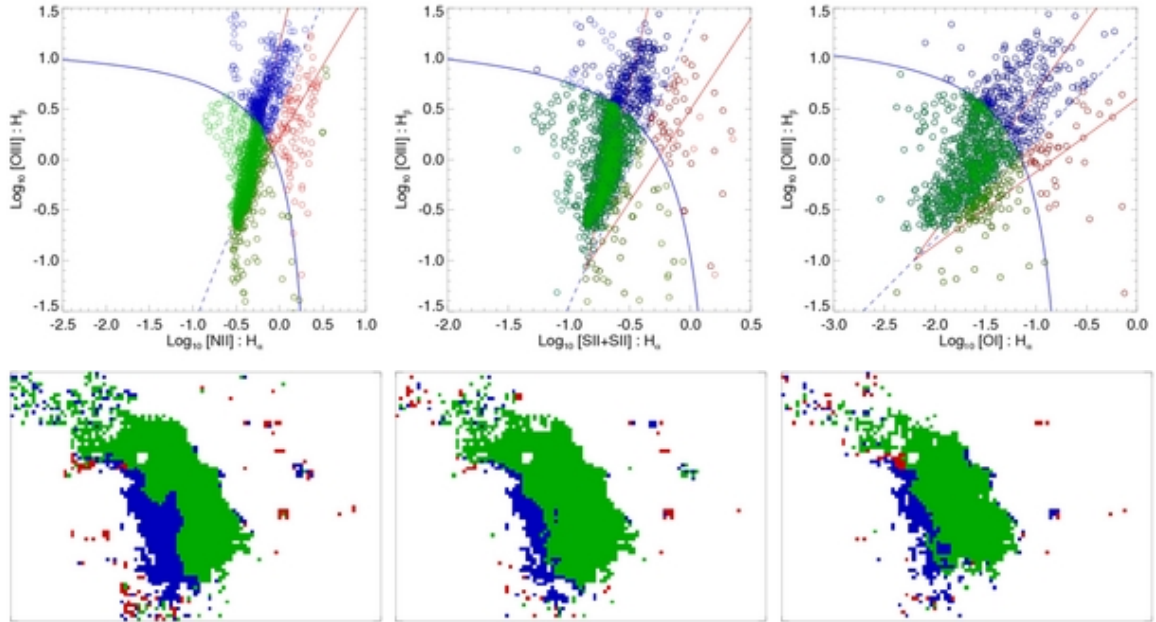
FIG. 18.— NGC 1365: Ionisation Diagnostic Diagrams are constructed following Fig. 4.

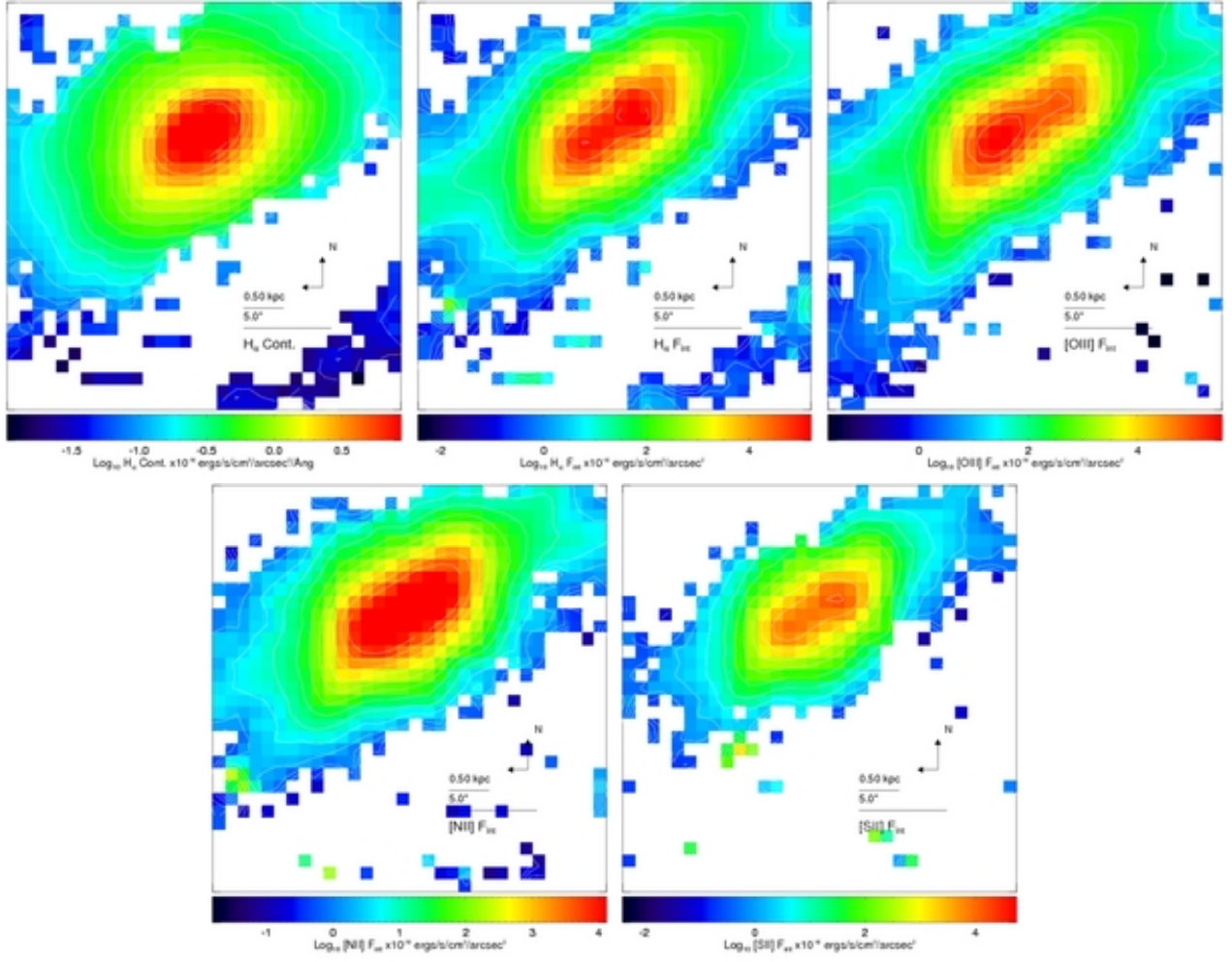FIG. 19.— Circinus: Emission line intensity maps following Fig. 2.

Fɪɢ. 20.— Circinus: Line ratio maps are constructed following Fig. 3.
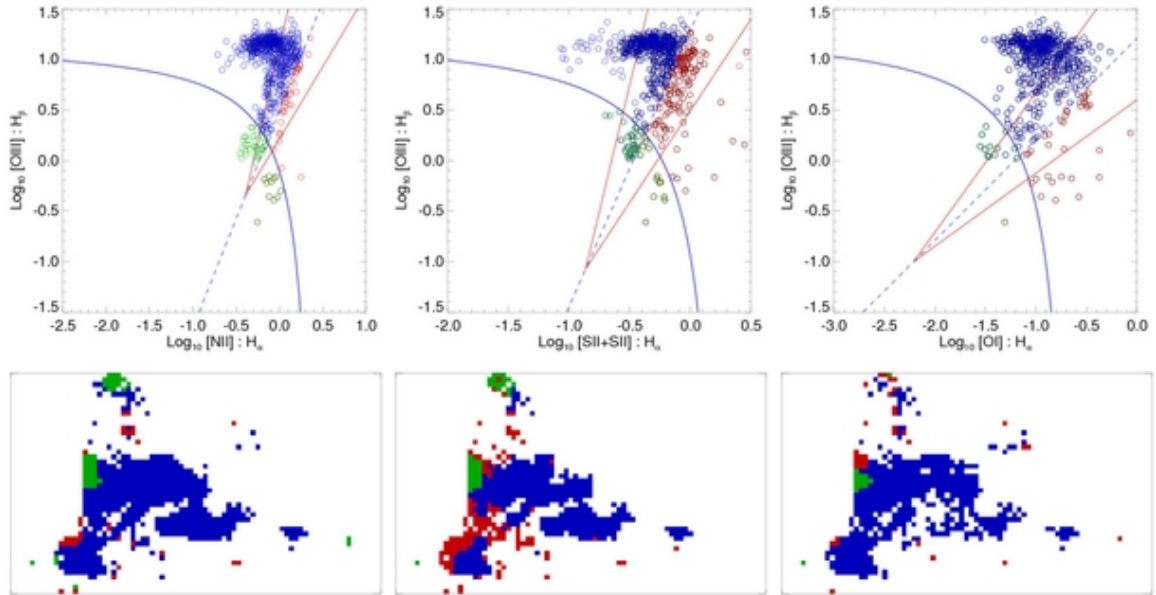
Fɪɢ. 21.— Circinus: Ionisation Diagnostic Diagrams are constructed following Fig. 4.
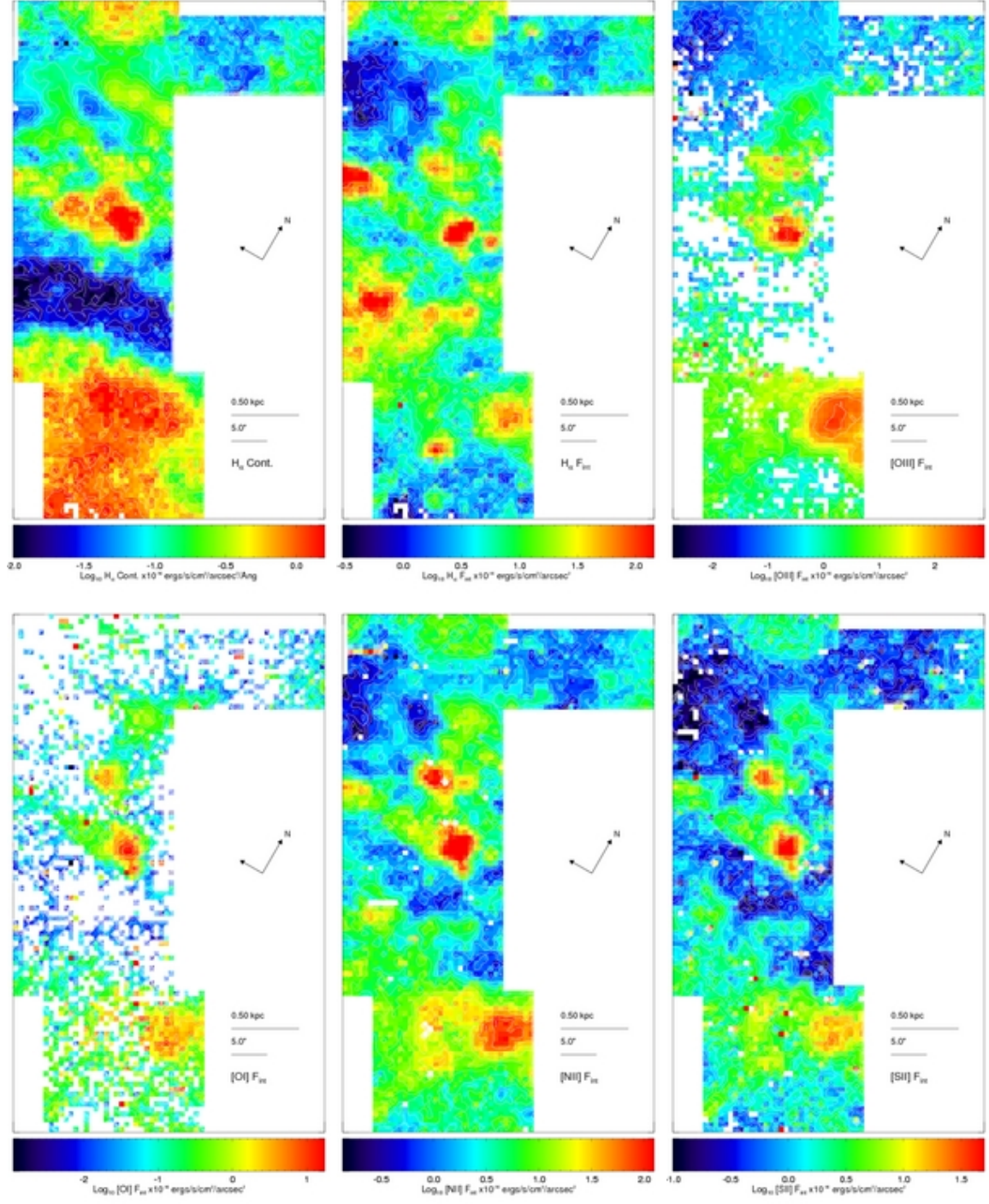
FIG. 22.— NGC 5128 (CenA): Emission line intensity maps following Fig. 2.

Sharp & Bland-Hawthorn
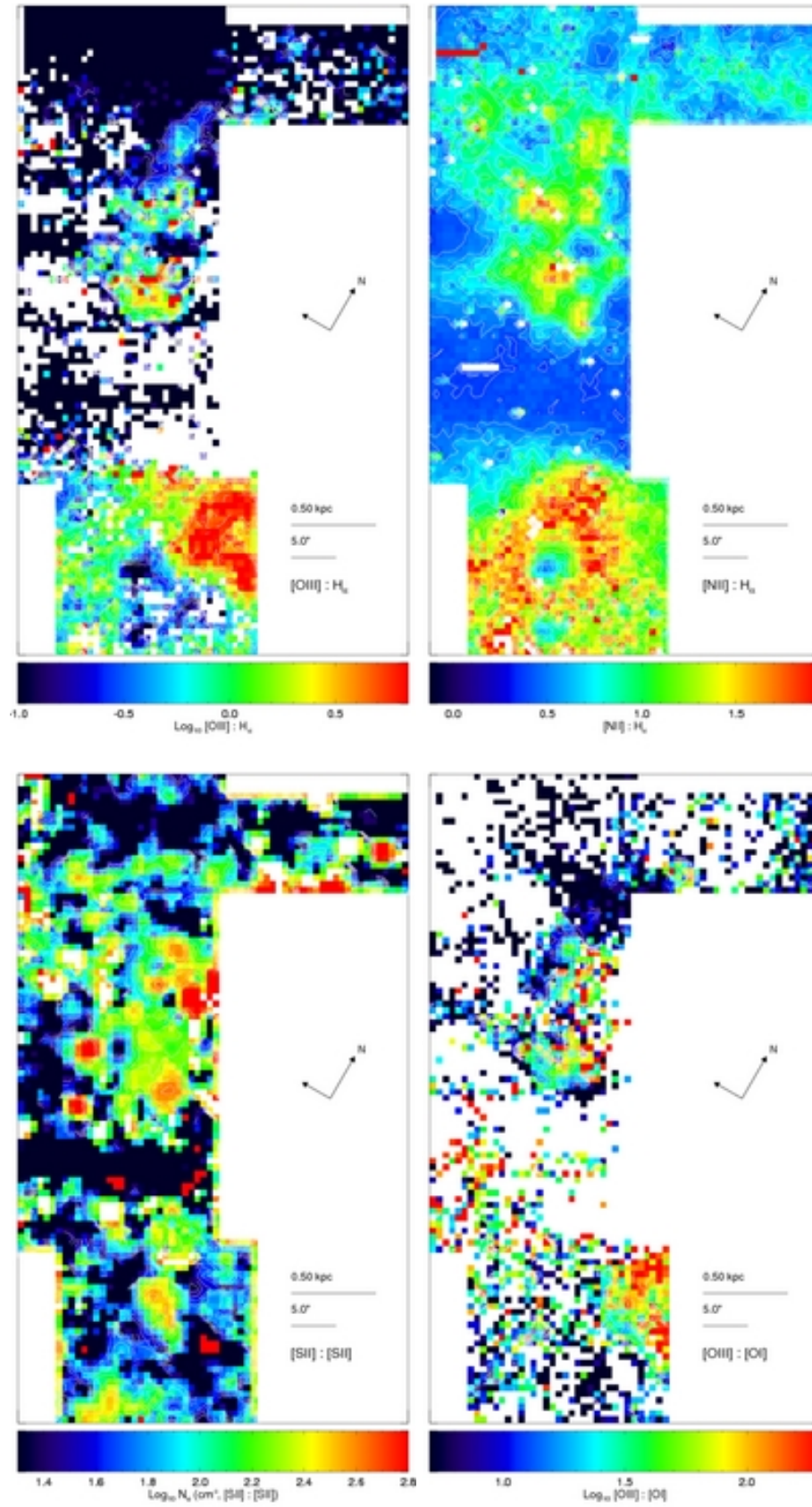
FIG. 23.— NGC 5128 (CenA): Line ratio maps are constructed following Fig. 3. Note the data cube was block averaged 3×3 prior to spectral fitting in the two [S II] lines for the construction of the electron density diagnostic due to the weak signal.
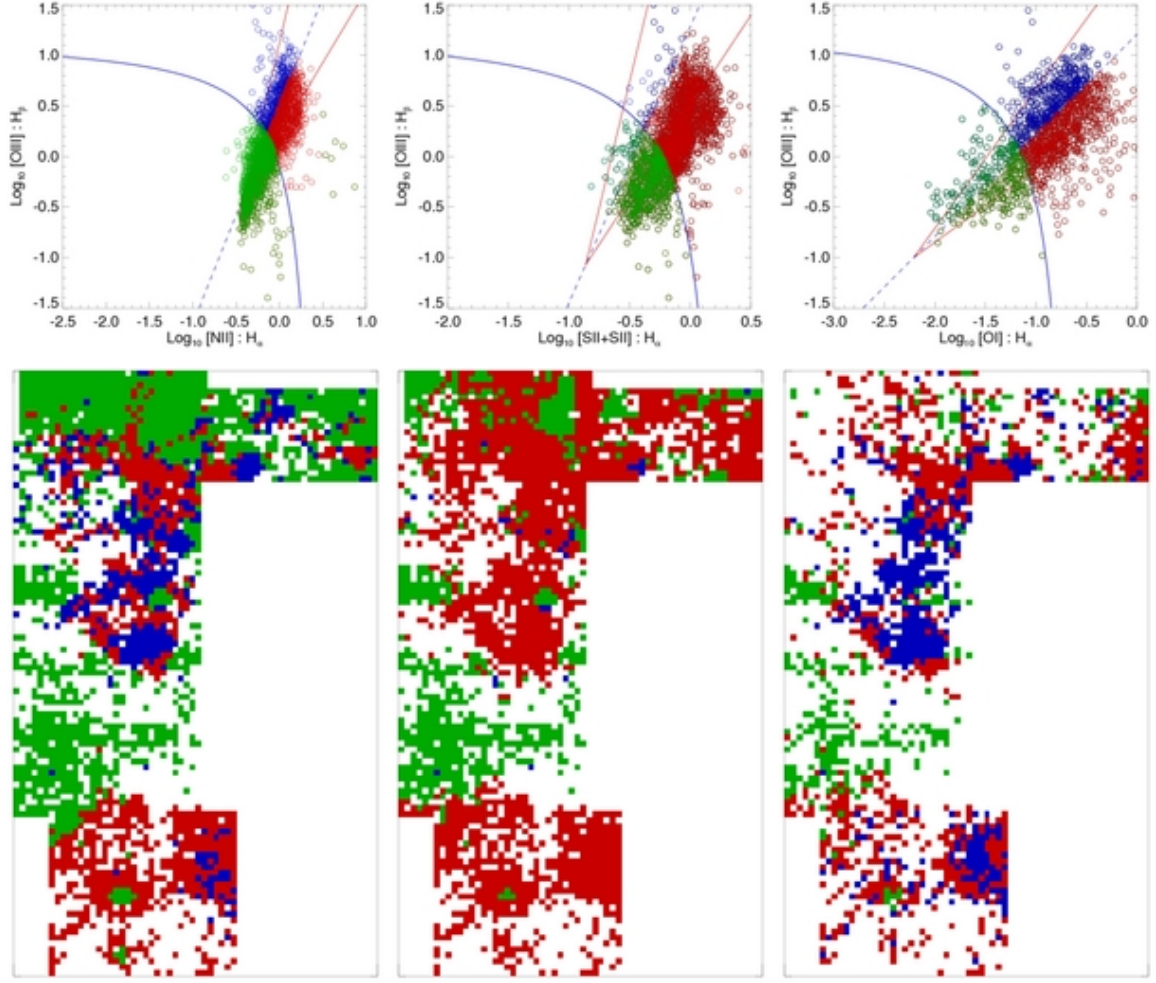
FIG. 24.— NGC 5128 (CenA): Ionisation Diagnostic Diagrams are constructed following Fig. 4.
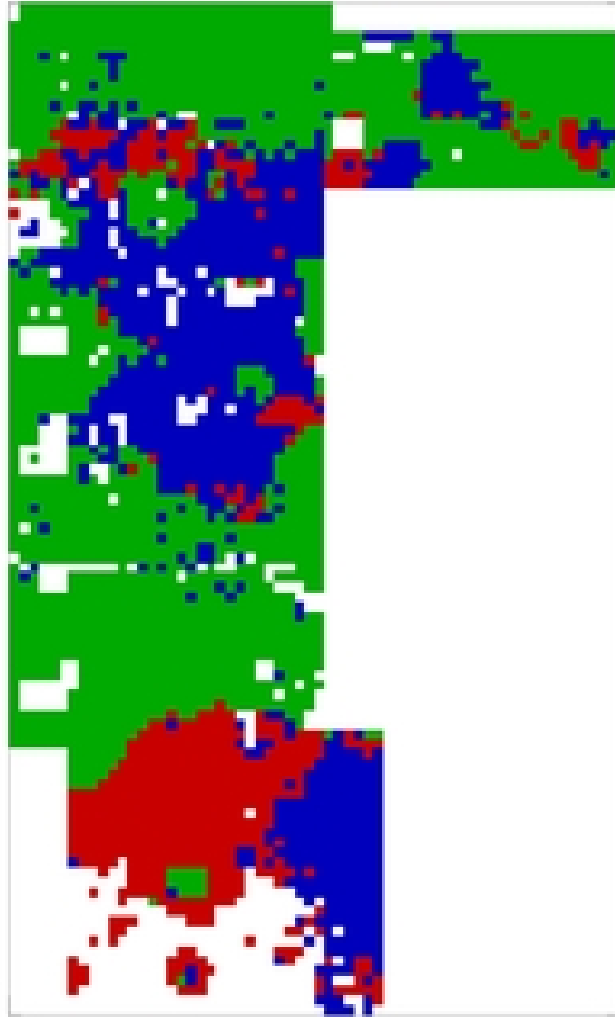
FIG. 25.— NGC 5128 (CenA): The ionisation cone due the hard AGN spectrum is revealed more clearly in the data after spatially re-binning the spectra 3×3. The classification scheme from the [O III]/Hβ vs. [N II]/Hα IDD (Fig. 24) is repeated here.

FIG. 26.— IC 5063: Emission line intensity maps following Fig. 2.
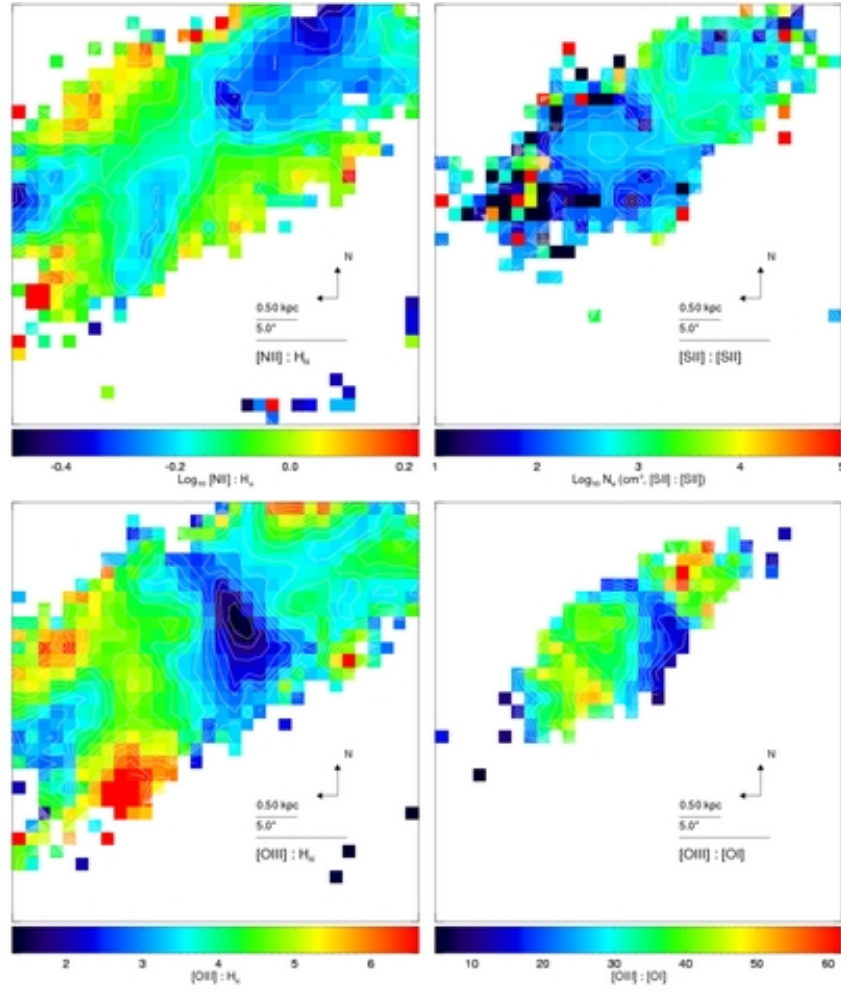
FIG. 27.— IC5063: Line ratio maps are constructed following Fig. 3.
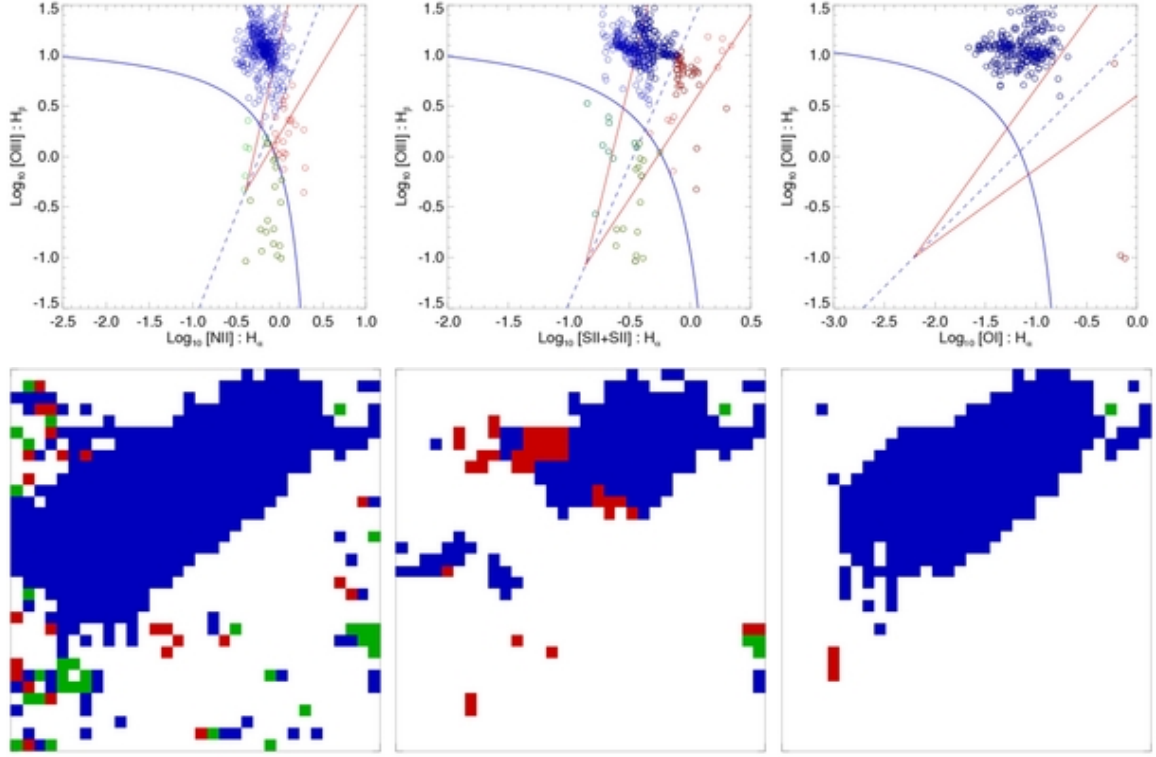
FIG. 28.— IC5063: Ionisation Diagnostic Diagrams are constructed following Fig. 4.
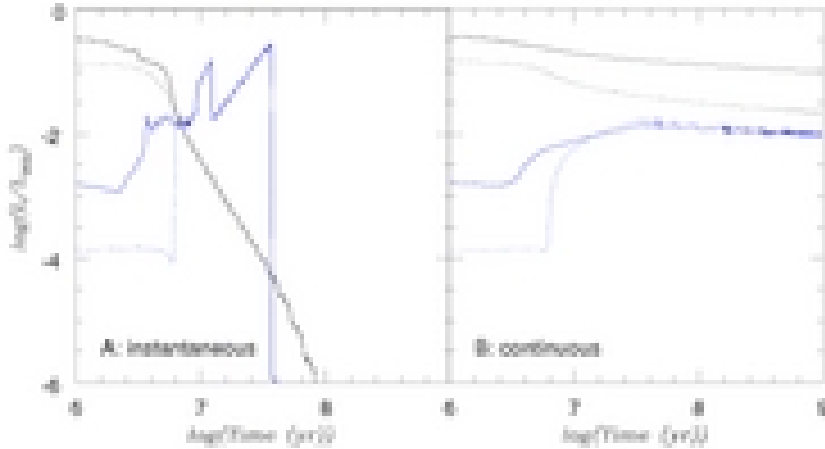
FIG. 29.— Ionizing luminosity (black) vs. mechanical luminosity (blue) evolution in two different star forming scenarios: (A) instantaneous burst; (B) continuous. In both cases, a Salpeter initial mass function is adopted but with two different upper mass cut-offs: 30 $M_\odot$ (dotted line), 100 $M_\odot$ (solid line).

APPENDIX

THE USE OF INTEGRAL FIELD SPECTROGRAPHS – LESSONS LEARNED

The use of a double-beam integral field spectrograph has been critical to the success of this project. It provides both detailed ionisation diagnostics and kinematics over the extent of the outflowing gas. We have demonstrated how these IDDs can be used to classify the nature of the wind outflow for each source, and to define spatial zones in which different ionisation sources dominate. Furthermore, we have begun the process of spectral and spatial kinematic and ionisation deconvolution for each source, in an effort to disentangle the complexity of each system.

We conclude that blue sensitivity (below 500nm) is a key factor to many of the diagnostic requirements, in particular sensitivity to the Hβ and [O III] spectral region (with SPIRAL we can not comment on the utility of [O II] emission feature for such work). As a clear shock diagnostic, [O I] is also of great value to classification of the nature of the ionisation source, although in all cases presented in this work, sensitivity to the [O III] emission still presents the primary limitation. This limitation is imposed in part by the reduced throughput of the blue arm of the AAOmega system (Sharp *et al.* 2006) but will remain an important consideration for more balanced systems.

Spectral resolution is critical to disentangling the multiple emission components of many of the sources discussed, with line splitting in many of the outflows only marginally resolved in our R$\sim$5000 spectroscopy ($\sim$50 km s^{-1}). One must of course also consider wavelength coverage. While many of the fainter lines common to ISM studies may be beyond the reach of a survey such as ours (for example the temperature sensitive [N II] $\lambda5756$ line is typically rather faint) we have demonstrated the added value of an extended spectral range in contrast to the limited coverage usually practical with Fabry-Pérot tunable filter systems such as that employed for example by Veilleux *et al.* (2003). A range of source redshifts, even for a nearby galaxy sample, further complicates the choice of wavelength range selection.

The observations and interpretation presented here have been possible primarily due to the high surface brightness sensitivity of the AAOmega-SPIRAL system afforded by the large projected spatial pixel size on the sky. The 0.7arcsec on a side square elements provide an individual field of view of 0.49arcsec^2, which represents factors of $\sim$2, 5.4 & 12 increase in contrast to 0.5,0.3 or 0.2arcsec systems, more than accounting for the smaller size of the prime mirror of the AAT 3.9m when compared to systems available on the current generation of large optical telescopes. This allows SPIRAL to move out of the detector readnoise limit, below which re-binning of adjacent apertures will not recover
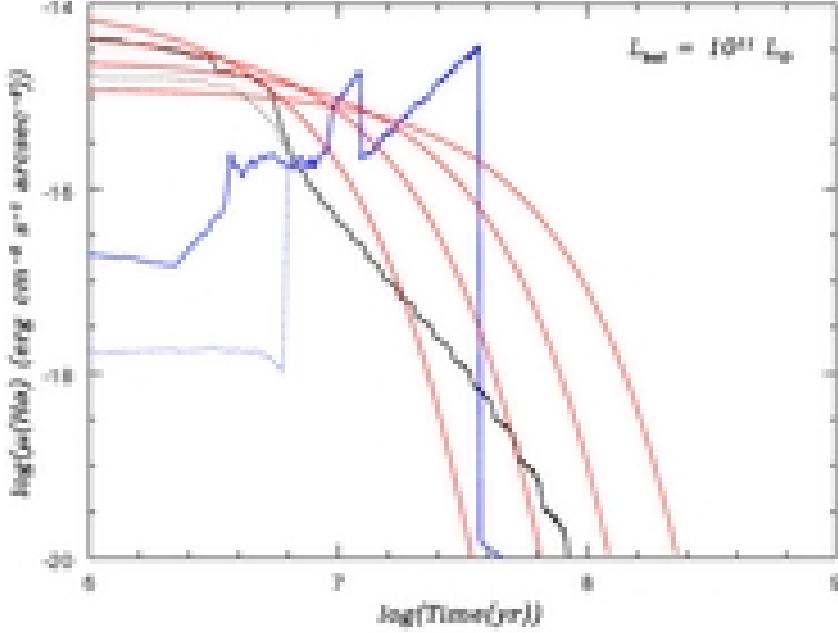
FIG. 30.— Predicted evolution of Hα surface brightness of optically thick gas at 1 kpc from a central active source with $L_{\rm bol} = 10^{11} L_{\odot}$. The black and blue curves are described in Fig. 29. The red curves correspond to 4 different sets of $(C_{\rm A,max}; t_A)$ in our AGN model, i.e. (0.1, 20), (0.2, 10), (0.4, 5), (0.8, 2.5) where the second value in each pair is the exponential timescale in Myr; larger values therefore produce slower decays. The predicted values are at least an order of magnitude higher than what we observe as we discuss in §4. We do not include the evolution of the AGN's mechanical luminosity for comparison because this is highly uncertain. But since AGN photoionization seems to dominate over shocks, we must assume that the mechanical luminosity profile falls below the AGN UV curve at all times and therefore does not resemble the starburst profile.

signal-to-noise quickly. As recently demonstrated by Westmoquette *et al.* 09a/b, in truth one must ultimately combine the wide field of view and low surface brightness observations practicable with large pixels, with dedicated narrow field observations at higher spatial resolution of critical regions of each object.